Article

Cell

Astrocytic Activation Generates *De Novo* Neuronal Potentiation and Memory Enhancement

Graphical Abstract

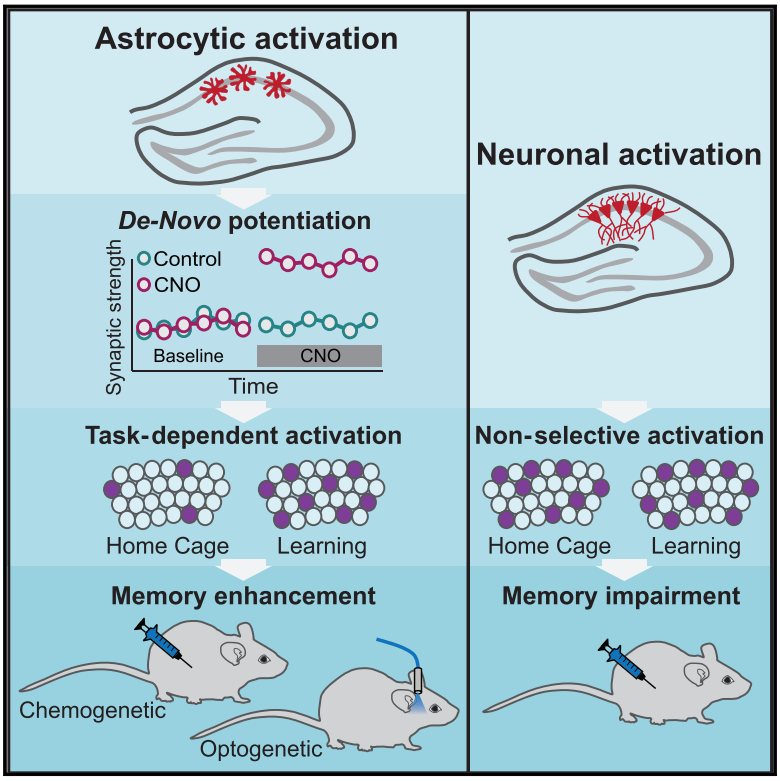

Authors

Adar Adamsky, Adi Kol, Tirzah Kreisel, ..., Maya Groysman, Michael London, Inbal Goshen

Correspondence

inbal.goshen@elsc.huji.ac.il

In Brief

Astrocyte activation in the hippocampus is sufficient to generate synaptic potentiation, enhance memory allocation, and improve cognitive performance beyond what can be achieved by elevating neuronal activity alone.

Highlights

- Astrocytic activation induces *de novo* NMDA-dependent long-term potentiation in CA1
- Chemogenetic activation of astrocytes, but not neurons, enhances memory acquisition
- Astrocytic, but not neuronal, activation specifically promotes memory allocation
- Optogenetic activation of the Gq-pathway in astrocytes augments memory acquisition

Adamsky et al., 2018, Cell *174*, 1–13
June 28, 2018
https://doi.org/10.1016/j.cell.2018.05.002

CellPress

Please cite this article in press as: Adamsky et al., Astrocytic Activation Generates *De Novo* Neuronal Potentiation and Memory Enhancement, Cell (2018), https://doi.org/10.1016/j.cell.2018.05.002

Article

Cell

Astrocytic Activation Generates *De Novo* Neuronal Potentiation and Memory Enhancement

Adar Adamsky,[1,4] Adi Kol,[1,4] Tirzah Kreisel,[1] Adi Doron,[1] Nofar Ozeri-Engelhard,[1] Talia Melcer,[1] Ron Refaeli,[1] Henrike Horn,[1] Limor Regev,[1] Maya Groysman,[2] Michael London,[1,3] and Inbal Goshen[1,5,*]

[1]Edmond and Lily Safra Center for Brain Sciences (ELSC), The Hebrew University of Jerusalem, Jerusalem 91904, Israel
[2]ELSC Vector Core Facility, The Hebrew University of Jerusalem, Jerusalem 91904, Israel
[3]Alexander Silberman Institute of Life Sciences, The Hebrew University of Jerusalem, Jerusalem 91904, Israel
[4]These authors contributed equally
[5]Lead Contact
*Correspondence: inbal.goshen@elsc.huji.ac.il
https://doi.org/10.1016/j.cell.2018.05.002

SUMMARY

Astrocytes respond to neuronal activity and were shown to be necessary for plasticity and memory. To test whether astrocytic activity is also sufficient to generate synaptic potentiation and enhance memory, we expressed the Gq-coupled receptor hM3Dq in CA1 astrocytes, allowing their activation by a designer drug. We discovered that astrocytic activation is not only necessary for synaptic plasticity, but also sufficient to induce NMDA-dependent *de novo* long-term potentiation in the hippocampus that persisted after astrocytic activation ceased. *In vivo*, astrocytic activation enhanced memory allocation; i.e., it increased neuronal activity in a task-specific way only when coupled with learning, but not in home-caged mice. Furthermore, astrocytic activation using either a chemogenetic or an optogenetic tool during acquisition resulted in memory recall enhancement on the following day. Conversely, directly increasing neuronal activity resulted in dramatic memory impairment. Our findings that astrocytes induce plasticity and enhance memory may have important clinical implications for cognitive augmentation treatments.

INTRODUCTION

Memory stands at the heart of cognitive function, guiding future behavior based on past experience. Memory disruption is relatively easy to induce, whereas memory enhancement has challenged scientists for many years. The majority of cognitive enhancement models involve alterations in synaptic function, often via direct or indirect effects on NMDA-R signaling (Lee and Silva, 2009). Another way to improve memory is to boost the process of memory allocation, the selection of the neuronal ensemble that will serve as the physical basis underlying the specific memory (Han et al., 2007; Josselyn et al., 2015; Yiu et al., 2014).

Although the supportive roles of astrocytes are well recognized, their direct effects on neuronal activity remain elusive. Pioneering studies have examined how astrocytes monitor and directly modulate neuronal activity, and support the idea of a "tripartite synapse," in which astrocytes do not merely encapsulate and insulate synapses, but also sense and actively modify synaptic activity (Araque et al., 1999; Haydon, 2001). Most of these studies were conducted on a single cell level, for example, by patching a single astrocyte to modulate its activity (Henneberger et al., 2010; Jourdain et al., 2007; Panatier et al., 2011) or by uncaging Ca^{2+} in single astrocytes (Perea and Araque, 2007). These techniques cannot be used in behaving animals, where modulating the activity of a population of astrocytes is required (Adamsky and Goshen, 2017; Dallérac and Rouach, 2016; Oliveira et al., 2015). Because of this difficulty, only a handful of studies have directly investigated the necessity of astrocytes in mammalian normal memory (Gao et al., 2016; Gerlai et al., 1995; Newman et al., 2011; Nishiyama et al., 2002; Stehberg et al., 2012; Suzuki et al., 2011; Tadi et al., 2015).

The studies above elegantly show that astrocytes are necessary for long-term plasticity and normal memory performance, but it is unknown whether astrocytic activity is not only necessary but also sufficient to induce synaptic plasticity and enhance cognitive performance. Beyond the clinical implications of memory enhancement, such an investigation could illuminate the complex way in which astrocytes do not merely respond to the neighboring neural network activity and support it, but rather precisely modulate the way it processes information.

To explore the role of astrocytes in synaptic activity and plasticity, as well as in memory performance, we employed chemogenetic and optogenetic tools in this cell population and found that astrocytic activation resulted in increased spontaneous vesicle release, and *de novo* synaptic potentiation mediated by NMDA. These plastic changes resulted in enhanced memory allocation and improved cognitive performance, which could not be directly achieved by elevating neuronal activity.

RESULTS

Chemogenetic Activation of CA1 Astrocytes

Based on the ability of endogenous Gq-GPCRs to induce Ca^{2+} elevation in astrocytes (Bazargani and Attwell, 2016) and their

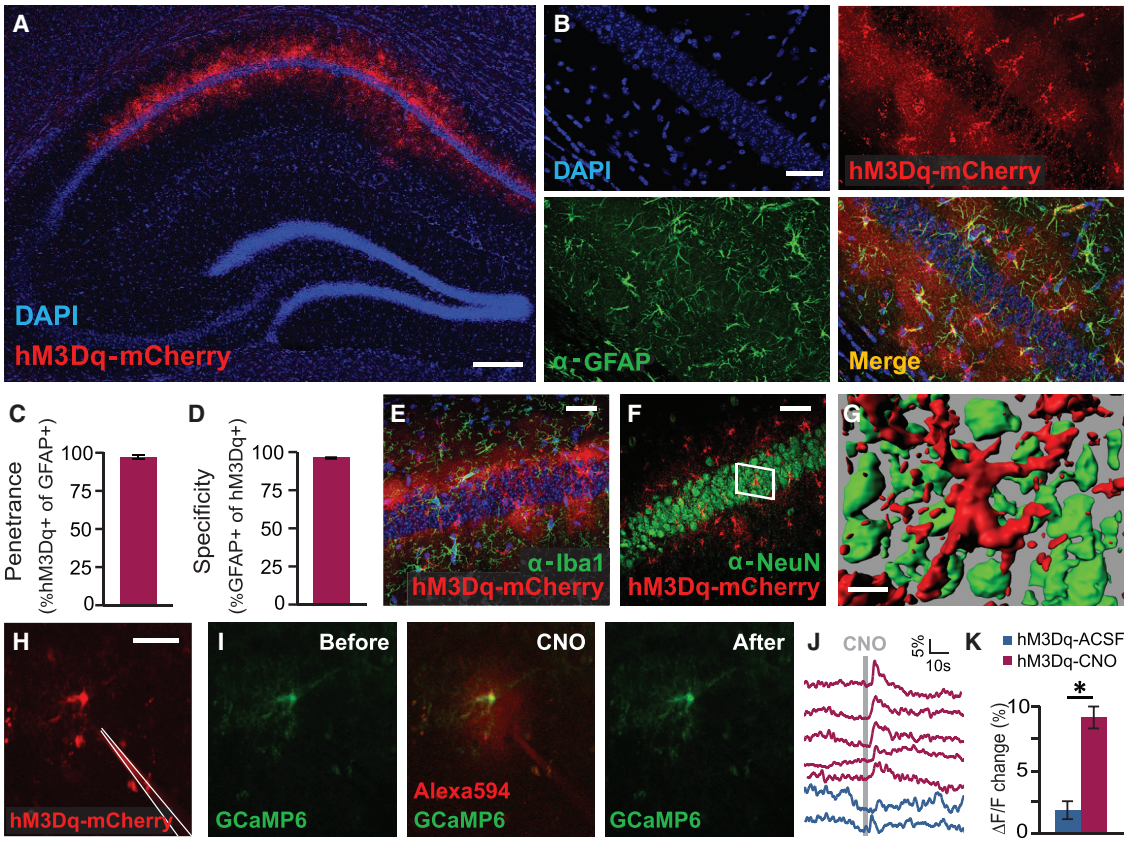

Figure 1. Chemogenetic Activation of Hippocampal Astrocytes

(A) Bilateral double injection of AAV8-GFAP::hM3Dq-mCherry resulted in hM3Dq expression in CA1 only (scale bar, 200 μm).

(B) hM3Dq (red) was expressed in the astrocytic membrane around the soma and in the distal processes (scale bar, 50 μm).

(C and D) GFAP::hM3Dq was expressed in >97% of CA1 astrocytes (408/419 cells from 3 mice; C), with >97% specificity (408/419 cells from 3 mice; D).

(E and F) No co-localization with the microglia marker Iba1 (E) or the neuronal nuclear marker NeuN (F) was detected (scale bar, 50 μm).

(G) An astrocyte (marked by a white rectangle in F) expressing hM3Dq in close proximity to multiple CA1 neurons (scale bar, 7 μm).

(H) Two-photon imaging of an hM3Dq-expressing astrocyte, with an adjacently placed glass pipette (scale bar, 20 μm).

(I) Local CNO administration via the glass pipette containing Alexa 594 (red) in the vicinity of the same astrocyte induced an increase in intracellular Ca^{2+}.

(J) Traces showing the change in fluorescence (in Δf/f) from hM3Dq-expressing astrocytes treated with CNO (crimson) or ACSF (blue). A gray line represents the 200 ms of CNO application. The top trace is from the astrocyte shown in (H) and (I).

(K) Summary of the results from all imaged cells (CNO n = 5 cells, ACSF n = 2 cells, from 3 mice) showing a significant increase in CNO-treated cells only (*$p < 0.005$). Data are presented as mean ± SEM.

See also Figure S1.

importance in neuron-astrocyte communication (Agulhon et al., 2008, 2013; Araque et al., 2014; Bonder and McCarthy, 2014; Bull et al., 2014; Chai et al., 2017; Chen et al., 2016; Martin-Fernandez et al., 2017; Scofield et al., 2015; Yang et al., 2015), we chose to express the Gq-coupled designer receptor hM3Dq (Roth, 2016) in CA1 astrocytes, allowing their time-restricted activation by clozapine-N-oxide (CNO). As the CA1 region of the hippocampus has been repeatedly shown to be involved in contextual memory (Frankland and Bontempi, 2005), and neurons in this region have demonstrated learning-dependent potentiation (Whitlock et al., 2006), we delivered an adeno-associated virus serotype 8 (AAV8) vector encoding hM3Dq fused to mCherry under the control of the astrocytic glial fibrillary acidic protein (GFAP) promoter (AAV8-GFAP::hM3Dq-mCherry) to this region (Figure 1A). Within the virally transduced region, hM3Dq expression was limited to the astrocytic outer membranes (Figure 1B), with high penetrance (>97% of the GFAP cells expressed hM3Dq) (Figure 1C) and almost complete specificity (>97% hM3Dq positive cells were also GFAP positive) (Figure 1D). Co-staining with the microglial marker Iba1 showed no overlap with hM3Dq expression (Figure 1E). The staining for neuronal nuclei (NeuN) revealed no co-localization with hM3Dq (Figure 1F), but served to illustrate how astrocytic processes within CA1 enwrap their neighboring neurons (Figure 1G).

To verify that hM3Dq activates astrocytes upon CNO application, we performed two-photon calcium (Ca^{2+}) imaging in brain slices. CA1 astrocytes expressing both hM3Dq and GCaMP6f were identified, and a glass pipette was placed adjacent to locally apply CNO (10 mM) (Figure 1H). CNO application triggered an intracellular Ca^{2+} increase in hM3Dq-expressing

astrocytes, whereas artificial cerebro spinal fluid (ACSF) application had no effect ($p < 0.005$, t test) (Figures 1I–1K). To characterize the effects of CNO application on astrocytic activity over longer time durations, relevant for upcoming slice and *in vivo* experiments, we imaged brain slices with CA1 astrocytes co-expressing GCaMP6f and mCherry (Figures S1A and S1B) before and during CNO application (10 μM), and then after CNO washout (Figure S1C). CNO application to the imaging chamber induced a significant increase in the number of Ca^{2+} transients in hM3Dq-GCaMP6f astrocytes (Figures S1D and S1E) that lasted 40 min. After CNO washout, the transient frequency returned to baseline. Importantly, ACSF application to hM3Dq-GCaMP6f slices or CNO application to GCaMP6f-only slices had no effect on Ca^{2+} transients (time-by-group effect $F(4,74) = 2.73$, $p < 0.05$, post hoc pairwise comparisons CNO versus ACSF and GCaMP alone during manipulation $p < 0.005$ and $p < 0.001$, respectively; CNO manipulation versus CNO baseline and CNO washout $p < 0.005$ and $p < 0.0005$, respectively). To conclude, hM3Dq is specifically expressed in CA1 astrocytes and can trigger an increase in intracellular Ca^{2+} and in the frequency of Ca^{2+} events, two markers for astrocytic activity (Bazargani and Attwell, 2016), upon CNO application.

Gq Pathway Activation in Astrocytes Increased the Frequency and Potency of Spontaneous Synaptic Events

Manipulations of single astrocytes have been employed in the past to show their involvement in spontaneous release events (Araque et al., 1998; Jourdain et al., 2007; Santello et al., 2011) and in excitatory post-synaptic potential (EPSP) induction success rate of minimal stimulation in the hippocampus (Panatier et al., 2011; Perea and Araque, 2007). Specifically, astrocytic inhibition resulted in more EPSP failures (Panatier et al., 2011), whereas astrocytic activation increased both the frequency of miniature spontaneous events and the responses to minimal stimulation (Jourdain et al., 2007; Perea and Araque, 2007), with no effect on amplitude, suggesting an exclusive pre-synaptic influence. To examine the effect of Gq pathway activation restricted to CA1 astrocytes on spontaneous synaptic release, we performed whole-cell recordings from CA1 hippocampal neurons in mice expressing hM3Dq in CA1 astrocytes (Figure 2A). Recordings were performed at a depth of ~100 μm in the slice, where the full structure of both the recorded neuron and the surrounding astrocytes is preserved. We recorded spontaneous release events in voltage clamp under tetrodotoxin (TTX) (1 μM) before and after bath application of CNO (10 μM), and found that CNO application resulted in increased frequency of miniature excitatory post-synaptic currents (mEPSCs) (Figures 2B–2E, S2A, and S2B; $p < 0.00001$, Kolmogorov-Smirnov test, and $p < 0.00001$, t test for the average change per cell). Importantly, astrocytic activation also induced a significant increase in mEPSC amplitude (Figures 2B, 2C, 2F, 2G, S2C, and S2D; $p < 0.0001$, Kolmogorov-Smirnov test, and $p < 0.01$, t test for the average change per cell), compared to slices from the same mice treated with ACSF only. To verify that CNO application itself does not produce similar effects, we injected mice with a control virus (AAV8-GFAP::mCherry) (Figure S2E). In hippocampal slices from these mice, neither ACSF nor CNO had an effect on mEPSC frequency (Figures S2F and S2G) or amplitude (Figures S2H and S2I).

We provide the first demonstration that astrocytic population activation increases both the rate and the potency of spontaneous miniature events impinging on CA1 pyramidal cells. It is possible that by using stimulation that more closely mimics physiological astrocytic activity, compared to repeated electrical depolarizations (Jourdain et al., 2007) or mechanical stimulation (Araque et al., 1998), we have been able to unveil the more subtle amplitude potentiation effect.

Gq Pathway Activation in Astrocytes Induced *De Novo* Synaptic Potentiation

The necessity of astrocytes in neuronal plasticity was repeatedly demonstrated in brain slices (Henneberger et al., 2010; Min and Nevian, 2012; Pascual et al., 2005; Perea and Araque, 2007; Suzuki et al., 2011) and *in vivo* (Chen et al., 2012; Navarrete et al., 2012; Takata et al., 2011). Furthermore, Ca^{2+} uncaging in astrocytes combined with post-synaptic depolarization (but neither of these manipulations alone) has been reported to induce long-term potentiation (LTP) (Perea and Araque, 2007), and repeated depolarization of DG astrocytes increased evoked EPSCs amplitude in granular neurons (Jourdain et al., 2007). We examined the effect of astrocytic Gq activation on evoked synaptic events in CA1 neurons in response to Schaffer collaterals (SCs) stimulation before and after bath application of CNO (Figures 3A and 3B). Surprisingly, we observed a 50% potentiation of the EPSC amplitude in response to the same stimulus in GFAP::hM3Dq slices treated with CNO (crimson), but not in slices from the same mice exposed to ACSF (blue) only (time-by-treatment interaction $F_{(19,190)} = 3.158$, $p < 0.00005$) (Figures 3C and 3D). To verify that this effect cannot be attributed to the application of CNO per se, we injected mice with a control AAV8-GFAP::mCherry virus (Figure S2E), and found no alteration in the response to stimulation before and after CNO application in slices from these mice (Figure S3A). To examine the long-term persistence of the observed potentiation, we tested the effect of astrocytic Gq activation on the evoked field potential in CA1 *stratum radiatum* to SC stimulation before, during, and after astrocytic activation (Figures 3E and 3F). We started by replicating our finding of *de novo* potentiation following astrocytic manipulation, now in the network level. This was shown by a greater than 150% increase in field EPSP (fEPSP) amplitude in response to a given stimulus in GFAP::hM3Dq slices treated with CNO, but not in ASCF-treated slices (Figures 3G–3I). We then washed the CNO out of the recording chamber for 20 min and measured fEPSPs for 10 more min. Evoked responses remained significantly potentiated in GFAP::hM3Dq slices that were previously treated with CNO, but not in ACSF-treated slices (Figures 3G–3I) (time-by-treatment interaction, $F_{(116,74.47)} = 3.16$, $p < 0.0000005$, Figure 3H; time-by-treatment interaction $F_{(8,34.87)} = 3.48$, $p < 0.005$, pairwise comparisons: CNO to baseline $p < 0.000005$, washout to baseline $p < 0.0005$, Figure 3I).

To perturb the mechanism underlying this long-term plasticity, we repeated the experiment with the NMDA receptor blocker APV (50 μM; green) applied to the recording chamber,

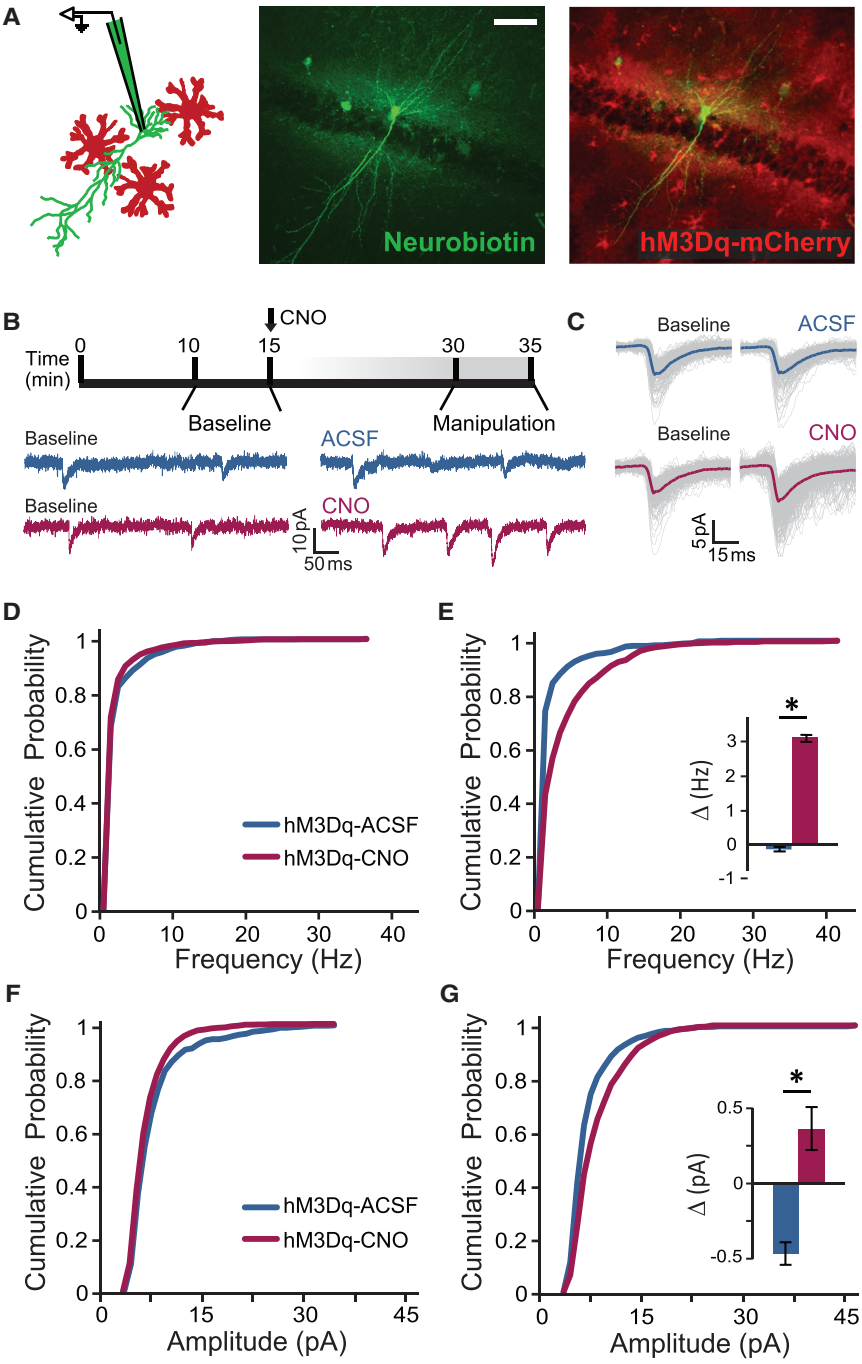

Figure 2. Astrocytic Activation Increases Spontaneous Neuronal Activity

(A) Whole-cell voltage-clamp recordings from CA1 hippocampal neurons (filled with Neurobiotin 488, green) surrounded by hM3Dq-expressing astrocytes (red; scale bar, 50 μm).

(B) Spontaneous miniature release events under TTX were recorded before and after CNO application (CNO, n = 6; ACSF, n = 3). Sample traces of an ACSF-only cell (blue) and a CNO-treated cell (crimson) are shown.

(C) Overlaid events from 5-min-long traces in two representative cells. Single events are in gray, and averages are bolded.

(D) No differences in mEPSCs frequency were observed between the groups before drug application.

(E) CNO application increased the frequency of spontaneous events, compared to ACSF alone ($p < 0.00001$). Inset: average change in frequency for all recorded cells (*$p < 0.00001$).

(F) No differences in mEPSC amplitude were observed between the groups before drug application.

(G) CNO application increased the mEPSC amplitude compared to ACSF alone ($p < 0.0001$). Inset: average change in amplitude for all recorded cells (*$p < 0.01$). Data are presented as mean ± SEM. See also Figure S2.

in which case CNO application failed to increase fEPSP size (Figures 3G–3I). Another demonstration of the involvement of NMDA in astrocyte-induced potentiation is the finding that in the presence of higher magnesium levels (2 mM, compared to 1 mM in the original experiment), more SC stimulations were necessary to reach the full potentiation effect (time effect, $F_{(3,8.1)} = 5.85$ $p < 0.02$, pairwise comparisons: baseline to CNO11-20 $p < 0.05$, baseline to CNO21-30 $p < 0.005$) (Figure S3B).

D-serine was shown to underlie the necessity of astrocytes to LTP (Henneberger et al., 2010). To resolve the role of D-serine in astrocyte-induced *de novo* potentiation, we used the NMDA D-serine site blocker 5,7-dichlorokynurenic acid (DCKA) (750 nM; cyan), which completely blocked potentiation (Figures 3G–3I). We then repeated the experiment in the presence of 10 μM D-serine in the bath and found that when the D-serine co-agonist site was highly occupied, the effect of CNO was occluded, and no potentiation was observed (Figure S3C).

We subsequently tested the role of metabotropic glutamate receptors (mGluRs) in astrocyte-induced synaptic potentiation, and found that the CNO application significantly potentiated fEPSPs even in the presence of the mGluRs blockers 2-methyl-6-(phenylethynyl)pyridine (MPEP, 50 μM) and LY367385 (100 μM) (Figures 3G–3I, orange), suggesting no contribution of mGluRs in the observed potentiation (pairwise comparisons: CNO to baseline $p < 0.0005$, washout to baseline $p < 0.01$) (Figure 3I).

Finally, to confirm that synaptic potentiation induced by astrocytic activation is mediated by an increase in astrocytic intracellular Ca^{2+} levels, we applied CNO after filling a group of astrocytes with the Ca^{2+} chelator EGTA and $CaCl_2$, to clamp intracellular free Ca^{2+} at a steady-state concentration

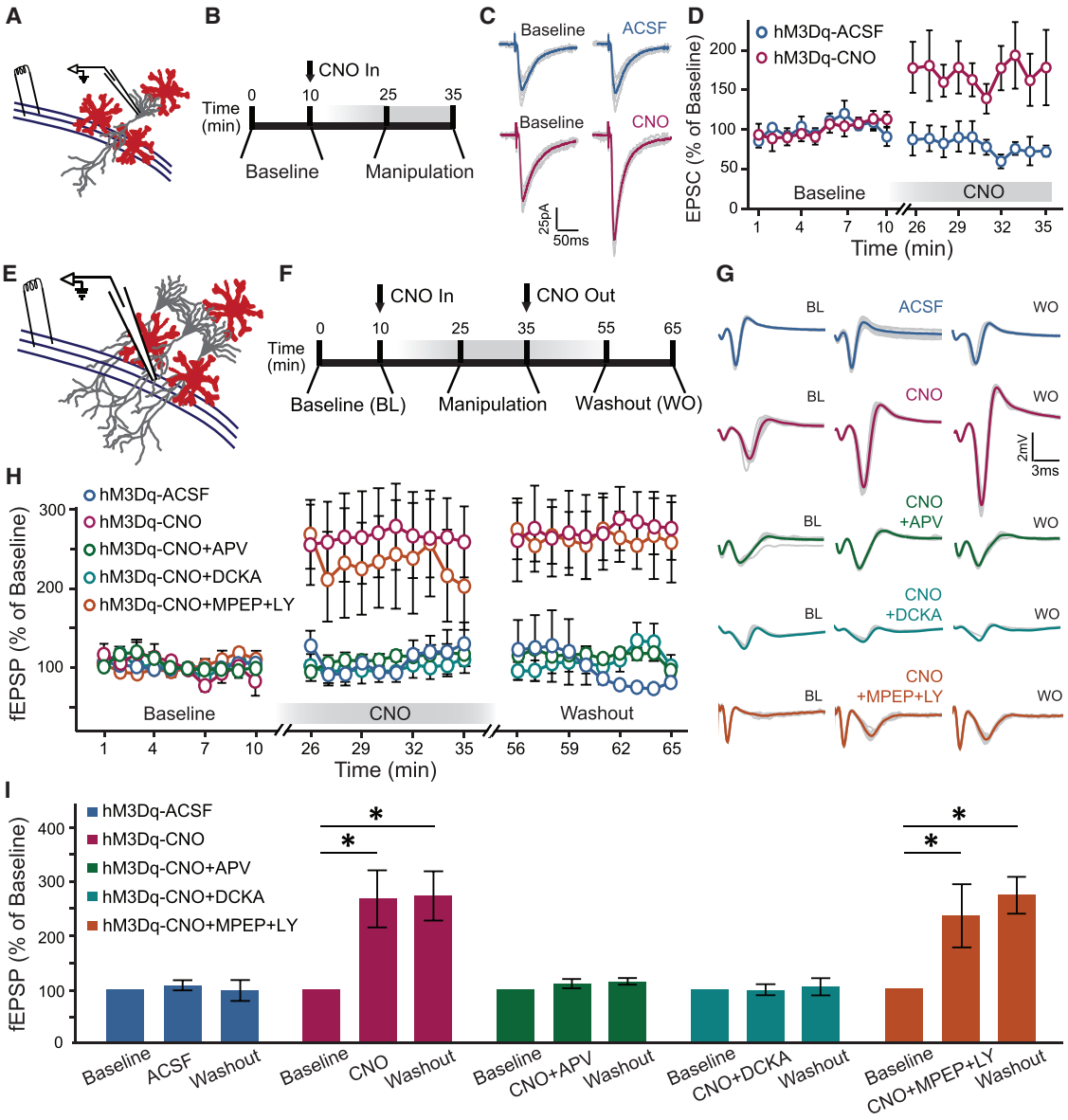

Figure 3. Astrocytic Activation Induces *De Novo* Plasticity

(A) Whole-cell voltage-clamp recordings from CA1 hippocampal neurons surrounded by hM3Dq-expressing astrocytes were performed in response to SC stimulation.

(B) Measurements were performed for 10 min at two time points: before CNO application or 15 min after CNO application.

(C) Overlaid evoked EPSCs from an ACSF-treated cell (blue) and a CNO-treated cell (crimson) before and after drug application are presented (single events are in gray; averages are bolded).

(D) No differences in evoked EPSCs amplitude were observed between the groups before drug application. Astrocytic activation by CNO induced a prolonged potentiation in evoked EPSC amplitude compared to slices from the same mice treated with ACSF (CNO, n = 8; ACSF, n = 4; $p < 0.00005$).

(E) Extracellular field recordings from the apical dendrites of CA1 hippocampal neurons surrounded by hM3Dq-expressing astrocytes were performed in response to SC stimulation.

(F) Measurements were performed for 10 min at three time points: before CNO application, 15 min after CNO application, and 20 min after CNO washout.

(G) Overlaid evoked fEPSPs from ACSF (blue), CNO (crimson), CNO+APV (green), CNO+CDKA (cyan), and CNO+MPEP+LY367385 (orange) treated slices before and after drug application and after drug washout.

(H) Astrocytic activation by CNO induced >150% potentiation in evoked fEPSP amplitude compared to slices from the same mice treated with ACSF. Application of the NMDA receptor blocker APV and the D-serine co-agonist site blocker DCKA completely eliminated the astrocyte-induced potentiation, but the mGluR blockers MPEP and LY367385 had no effect (CNO, n = 4–5; CNO+APV, n = 3; CNO+DCKA, n = 6; CNO+MPEP+LY, n = 4; ACSF, n = 2).

(I) Average representation of the data in (H) (CNO to baseline *$p < 0.00005$, CNO washout to baseline *$p < 0.0005$).

Pairwise comparisons: CNO+MPEP+LY to baseline *$p < 0.0005$, CNO+MPEP+LY washout to baseline *$p < 0.01$. Data are presented as mean ± SEM.

See also Figure S3.

of 50–80 nM (Figure S3D–S3G). fEPSPs recorded in adjacent neurons were only minimally potentiated compared to the significant potentiation observed in distant neurons (Figure S3H).

Here, we show, for the first time, that astrocytic activation is sufficient to induce *de novo* potentiation of CA3 to CA1 synapses, and that this potentiation is long lasting, beyond the time of astrocytic activation. The fact that our manipulation produced prolonged potentiation whereas Ca^{2+} uncaging in astrocytes required additional direct post-synaptic depolarization to induce LTP (Perea and Araque, 2007), may be due to the prolonged astrocytic activation in our experiments. Furthermore, we show that the synaptic potentiation induced by astrocytic activation is mediated by the NMDA receptor, similar to classical CA3 to CA1 LTP, and demonstrate the involvement of the NMDA co-agonist D-serine in this potentiation.

Astrocytic Activation Enhanced Spatial and Contextual Memory

Based on our finding that astrocytic activation is sufficient to induce neuronal potentiation, and on previous research demonstrating the necessity of astrocytes in memory function (Gerlai et al., 1995; Newman et al., 2011; Nishiyama et al., 2002; Stehberg et al., 2012; Suzuki et al., 2011; Tadi et al., 2015), we sought to test whether astrocytic activation can enhance memory performance. Mice were injected bilaterally with AAV8-GFAP::hM3Dq-mCherry to the dorsal CA1. To verify astrocytic activation *in vivo*, we administered CNO (3 mg/kg, intraperitoneally [i.p.]) 3 weeks after surgery, and brains were collected 90 min later and stained for the immediate-early gene cFos. CNO dramatically increased cFos levels in astrocytes of hM3Dq-expressing mice, compared to saline-injected controls (Figures 4A and 4B; $p < 0.0005$, t test). Fear conditioning (FC) exposure had no effect on cFos levels in astrocytes (Figure S4A).

To test the effect of astrocytic activation on cognitive performance, CNO was administered 30 min before T-maze training, in which mice were exposed to 2 arms of the maze for 20 min, and 5 min later were re-introduced to the maze, with all three arms now available for exploration. CNO application resulted in a significant elevation in novel arm preference compared to saline-injected controls (Figures 4C and 4D) ($p < 0.05$, t test). No effect of CNO on overall maze exploration was observed (Figure S4B). In this experiment, astrocytes were activated during both acquisition and recall, and could have contributed to cognitive enhancement at either stage.

To better define the memory stage affected by astrocytes, and extend our findings to an additional cognitive task, we administered CNO 30 min before FC training, pairing a foot-shock with a novel context and an auditory cue, in a new cohort of mice. No effect of CNO on exploration of the context before conditioning (Figure S4C) or immediate freezing following shock administration (Figure 4E) was observed. One day later, mice were placed back in the conditioning context, and freezing was measured. Remarkably, CNO application during training resulted in a 40% elevation in contextual freezing in GFAP::hM3Dq mice tested 24 hr after acquisition, when CNO was no longer present (Alexander et al., 2009) (Figure 4E; $p < 0.015$, t test). To establish the spatial specificity of our manipulation, we verified that the effect of CA1 astrocytic activation is unique to the hippocampal-dependent contextual memory task: Indeed, no effect was observed when the same mice were tested for auditory-cued memory in a novel context, i.e., both groups demonstrated similar freezing in response to the tone (Figure 4F) ($F_{(1,11)} = 106.04$, time main effect, $p < 0.00001$). CNO application during recall in the conditioning context on the next day did not further alter recall, but the original improvement was still evident (Figure 4G).

To further differentiate between the roles of astrocytes during acquisition and recall, we injected two new cohorts of mice with AAV8-GFAP::hM3Dq-mCherry to their CA1, and administered CNO 30 min before FC acquisition in one cohort, and 30 min before recall in the other. Importantly, in the first new cohort, we replicated our initial observation that astrocytic activation during acquisition enhanced recall on the next day (Figure S4E) ($p < 0.005$, t test), without affecting auditory-cued memory (Figure S4F) ($F_{(1,16)} = 47.57$, time main effect, $p < 0.00001$), or exploration of the chamber before conditioning (Figure S4D). In the second cohort, CNO was not administered during acquisition, but rather 30 min before the recall test. GFAP::hM3Dq mice injected with CNO at that time showed similar contextual (Figure 4H) and auditory-cued (Figure 4I) freezing, compared to saline controls. These findings suggest that astrocytes confer their cognition-enhancing effects during memory acquisition, and possibly early consolidation, but not during memory recall.

To verify that astrocytic activation does not have a direct effect on exploratory behavior or anxiety, which may result in increased freezing, we tested free exploration of an open field in the same GFAP::hM3Dq mice. CNO application had no significant effect on either total exploration or anxiety-related behavior, measured as the percent time spent in the central 35% of the arena (Figure 4J). To confirm that our results did not stem from the CNO application itself, we trained additional cohorts of mice, injected with a control AAV8-GFAP::eGFP vector (Figure S5A) in the same repertoire of behavioral paradigms. CNO application in these control mice had no effect on any behavior (Figures S5B–S5K).

Our behavioral results show that astrocytic activation during memory acquisition and early consolidation is sufficient to improve memory retrieval in two cognitive tasks.

Directly Increasing Neuronal Activity Impairs Contextual Memory

Our findings that astrocytic activation resulted in increased synaptic transmission, *de novo* plasticity and improved memory, raises the tempting hypothesis that astrocytes react to neuronal activity around them and modulate it in a physiologically meaningful way, leading to improved coding of contextual information. However, we cannot exclude the possibility that the observed memory enhancement could have been caused by a general increase in hippocampal neuronal activity induced by the manipulated astrocytes. To test whether directly increasing neuronal activity results in similar effects, we sought to stimulate CA1 neurons and test the consequent changes in cognitive performance. To that end, we injected mice with an AAV8 vector encoding hM3Dq-mCherry under the control of the CaMKIIα promoter,

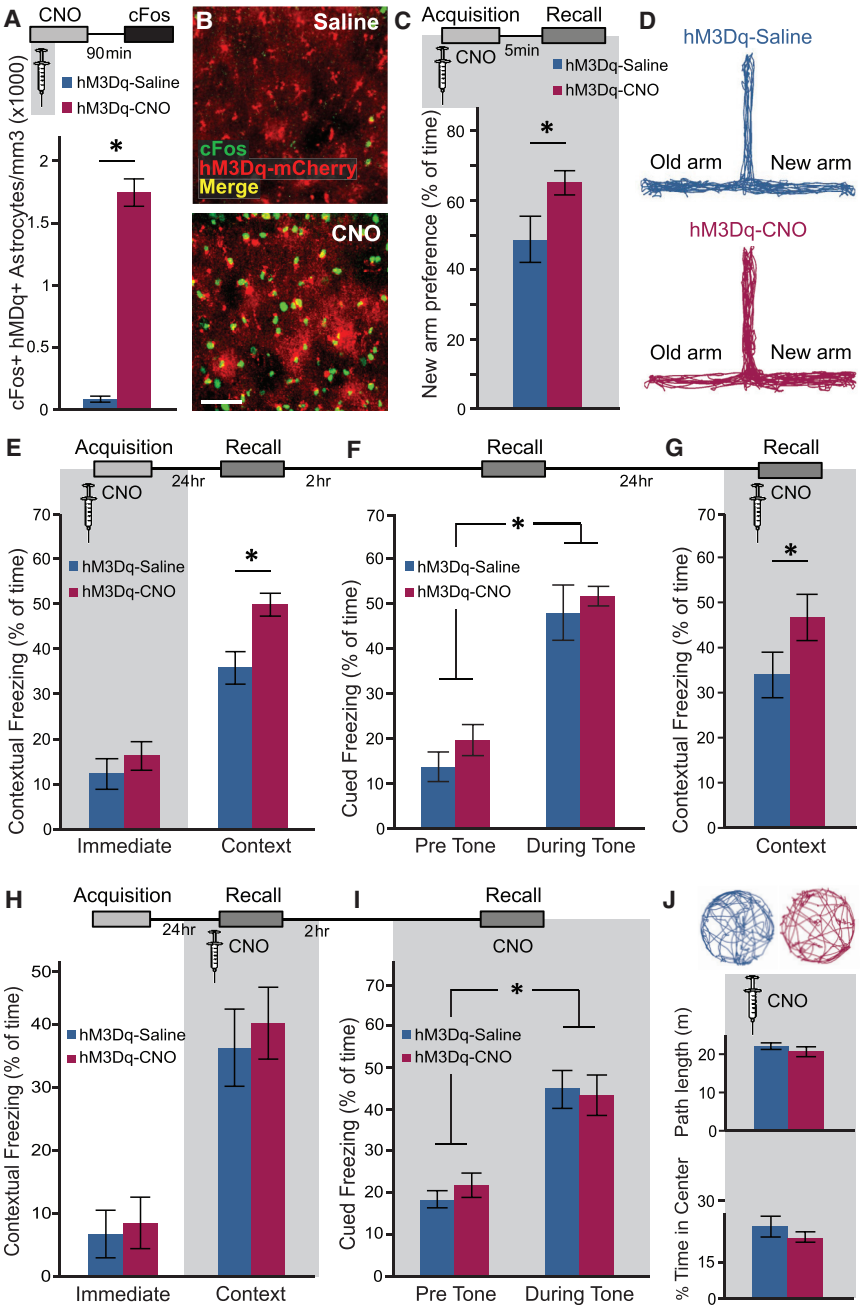

Figure 4. Astrocytic Activation Enhances Contextual Memory

(A and B) (A) CNO administration *in vivo* to mice expressing hM3Dq (red) in CA1 astrocytes resulted in a significant increase in cFos expression (green) in the activated astrocytes, compared to saline-injected controls (*$p < 0.0005$; n = 4 mice, 18 slices, for both groups; scale bar, 50 μm). (B) Representative images to the group data presented in (A).

(C) GFAP::hM3Dq mice that were injected with CNO (n = 7) 30 min before T-maze training demonstrated > 30% improved novel arm recognition (*$p < 0.05$) compared to their saline-injected controls (n = 7).

(D) Representative exploration traces.

(E) GFAP::hM3Dq mice were injected with saline (n = 6) or CNO (n = 7) 30 min before fear conditioning acquisition. CNO application before training resulted in a 40% improvement in contextual freezing in mice tested 1 day later, compared to saline-treated controls (*$p < 0.015$).

(F) Astrocytic activation in CA1 had no effect on auditory-cued memory in a novel context, with both groups showing increased freezing during tone presentation (*$p < 0.00001$).

(G) Astrocytic activation by CNO application during retrieval on the next day did not further alter recall, but the original improvement was maintained (*$p < 0.05$).

(H and I) In a new group of GFAP::hM3Dq mice, CNO administration (n = 7) only during the recall test had no effect on either contextually (H) or auditory-cued (I) memory, compared to saline-injected controls (n = 7) with both groups showing increased freezing during tone presentation (*$p < 0.000001$).

(J) In a novel environment, saline-treated (n = 6) and CNO-treated (n = 6) hM3Dq mice explored the field with similar path lengths (top), and there was no effect on anxiety (bottom), because the percentage of time that saline- and CNO-treated mice spent in the center of the open field was similar. Representative exploration traces are presented. Data are presented as mean ± SEM.

See also Figures S4 and S5.

specific to glutamatergic neurons. hM3Dq was shown in the past to increase firing, elevate fEPSP size and enhance LTP in CA1 pyramidal neurons, but it also poses a risk of seizures (Alexander et al., 2009; López et al., 2016). To avoid this risk, we aimed for a moderate expression level. Stereotactic delivery of the AAV8-CaMKIIα::hM3Dq-mCherry vector resulted in CA1-specific expression (Figure 5A). hM3Dq was exclusively expressed in neurons (Figure 5B) with moderate penetrance (47% of the NeuN cells expressed hM3Dq) and complete specificity (>98% hM3Dq-positive cells were also NeuN positive) (Figure 5C). Co-staining with the astrocytic marker GFAP or the microglial marker Iba1 showed no overlap with hM3Dq expression (Figures 5D and 5E). To test the effect of direct neuronal activation on memory acquisition, we injected CaMKIIα::hM3Dq mice with CNO (3 mg/kg, i.p.) 30 min before FC acquisition. First, we verified that this manipulation does not induce seizures or affect motor function, by quantifying the exploration of the conditioning cage during the 120 s before the introduction of the first tone. No difference between hM3Dq-mCherry mice treated with saline or CNO was observed (Figure 5F). Mice were then FC and tested on the next day. Interestingly, neuronal activation during training resulted in dramatically reduced, rather than improved, contextual freezing one day later (Figure 5G) ($p < 0.01$, t test). No significant effect on auditory-cued memory in a novel context was observed, as both groups demonstrated similar freezing in

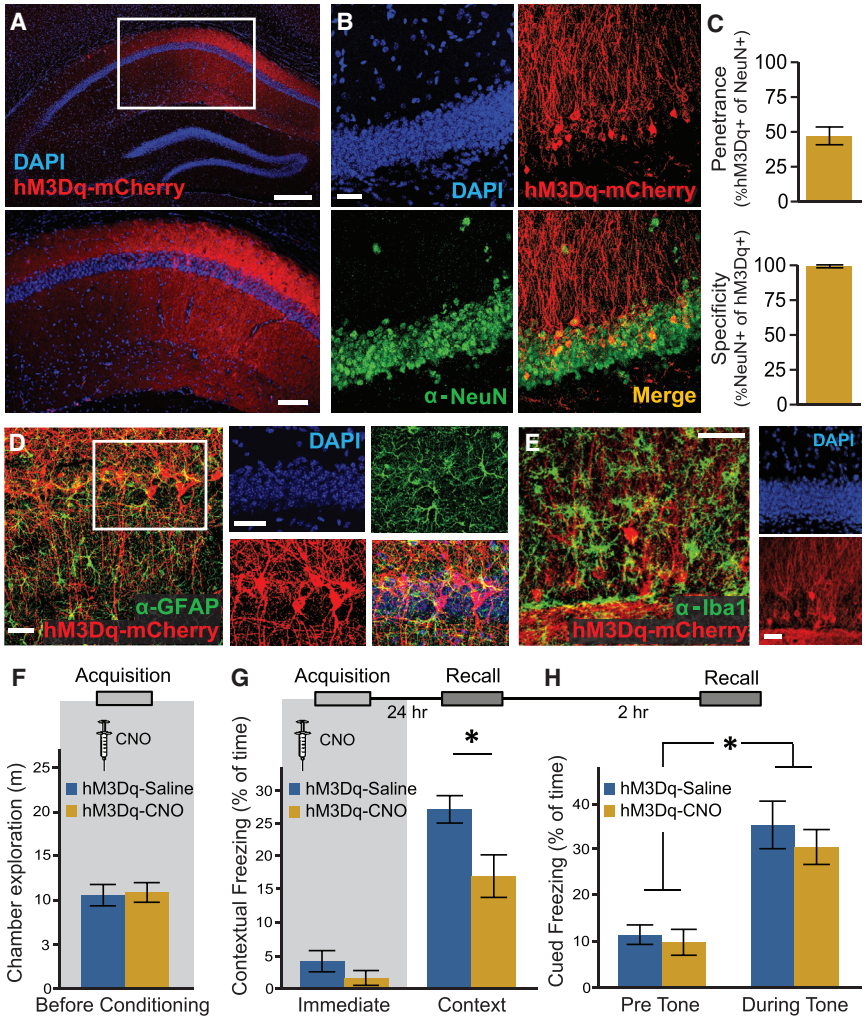

Figure 5. Neuronal Activation Impairs Memory Performance

(A) Bilateral double injection of AAV8-CaMKII::hM3Dq-mCherry resulted in relatively sparse hM3Dq expression in CA1 only (scale bar, top, 300 μm, and bottom, 100 μm).

(B) hM3Dq was expressed in the neuronal membrane around the soma and in the apical and the basal dendrites of CA1 neurons (scale bar, 30 μm).

(C) hM3Dq was expressed in 47% (442/913 cells, from two mice) of CA1 neurons, with >98% specificity (442/446 cells, from two mice).

(D and E) No co-localization with the astrocytic marker GFAP (D) or the microglial marker Iba1 (E) was detected (scale bar, 50 μm). Mice expressing hM3Dq in their CA1 neurons were injected with either saline (n = 9) or CNO (n = 8) 30 min before fear conditioning acquisition.

(F) Neuronal activation had no adverse effect on exploratory behavior in the conditioning cage.

(G) CNO application before training induced a 55% decrease in contextual freezing in CNO-treated mice tested 1 day later, compared to saline-treated controls (*$p < 0.01$).

(H) Neuronal activation in CA1 had no effect on auditory-cued freezing in a novel context, with both groups showing increased freezing during tone presentation (*$p < 0.00001$). Data are presented as mean ± SEM.

See also Figure S6.

response to the tone (Figure 5H) ($F_{(1,14)} = 48.165$, time main effect $p < 0.00001$).

We then replicated these results, this time manipulating a larger population of neurons, but activating them mildly, using a lower CNO dose (0.5 mg/kg) (Figure S6A). Again, no effects on context exploration before conditioning or immediate freezing following shock administration were observed (Figures S6B and S6C). Furthermore, neuronal activation with these new parameters during training again resulted in reduced contextual freezing a day later (Figure S6C) ($p < 0.05$, t test), and had no effect on auditory-cued memory in a novel context, as both groups demonstrated similar freezing in response to the tone (Figure S6D) ($F_{(1,10)} = 133.276$, time main effect $p < 0.00001$).

Here, we show that as opposed to astrocytic activation, which induces LTP and enhances FC performance, a direct chemogenetic stimulation of CA1 neurons dramatically impairs contextual memory.

Astrocytic Activation Promotes Memory Allocation

Our results show that astrocyte-mediated potentiation of neuronal activity enhances memory whereas direct neuronal activation dramatically impairs it. Previous research had demonstrated that a small number of neurons active before training are more likely to be allocated to the engram supporting an acquired memory (Josselyn et al., 2015), that such ensembles in CA1 are later necessary for recall (Tanaka et al., 2014) and that increasing the activity of a small neuronal population in the BLA before FC acquisition can improve fear memory (Han et al., 2007; Yiu et al., 2014).

Thus, we sought to test whether astrocyte-induced memory enhancement is not merely due to the general increase in neuronal activity, but rather stems from a tailored response of astrocytes to the activity of their surrounding neurons. To achieve that, we activated astrocytes or neurons *in vivo*, either in home-caged mice or in mice that acquired FC, and then measured cFos levels in CA1 neurons, as a marker for neuronal activity. Mice were bilaterally injected with AAV8-GFAP::hM3Dq-mCherry or AAV8-CaMKII::hM3Dq-mCherry or AAV8-GFAP::eGFP to the dorsal CA1, and 3 weeks later CNO (3 mg/kg, i.p.) was administered in the home-cage or 30 min before FC. Brains were collected 90 min later and stained for cFos (Figure 6A). FC increased cFos levels in all saline-injected mice (Figures 6B and 6C) ($p < 0.05$, t test). CNO administration to GFAP::hM3Dq mice *in vivo* increased neuronal activity beyond the threshold for cFos expression compared to saline-injected mice only when coupled with learning, but not in home-caged mice (Figures 6B and 6D) ($p < 0.05$, t test). CNO administration in

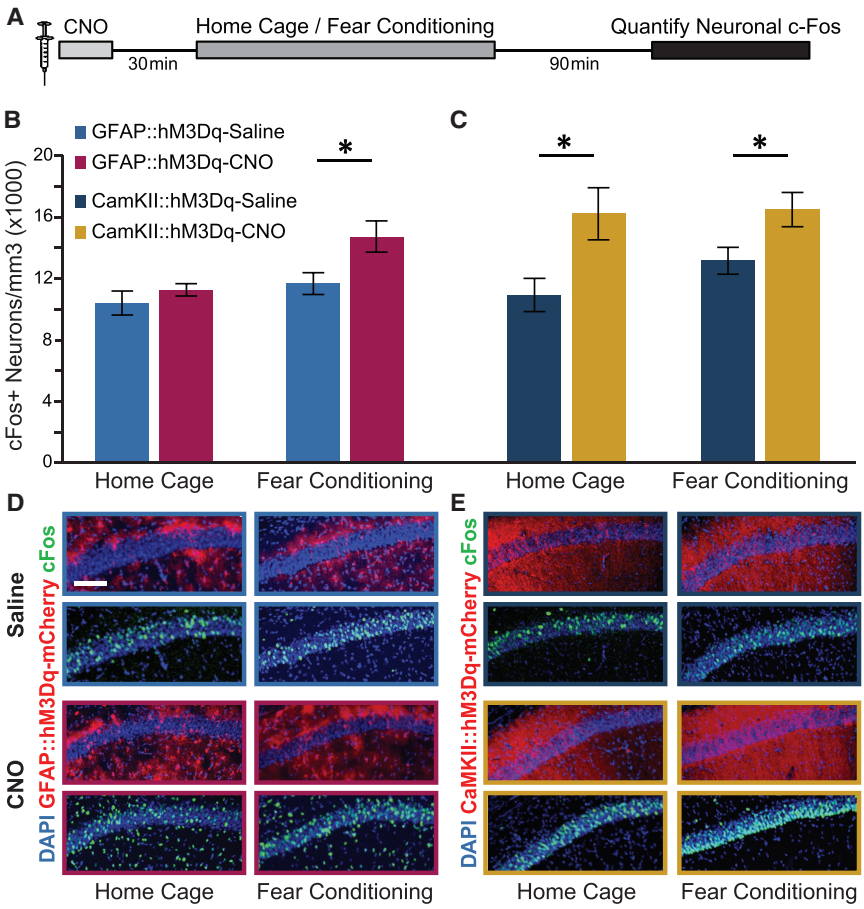

Figure 6. Astrocytic Activation Increases Neuronal Memory Allocation

(A) CNO was administered to mice injected with AAV8-GFAP-hM3Dq-mCherry or AAV8-CaMKII-hM3Dq. 30 min later, mice either underwent fear-conditioning acquisition or remained in their home cages. 90 min after that, brains were removed, sliced, and stained for cFos (n = 4–9 mice, 16–34 slices per group).

(B) CNO administration had no effect on neuronal cFos expression in GFAP::hM3Dq home-caged mice, but increased neuronal activity only when it was combined with fear memory acquisition (*$p < 0.05$).

(C) CNO administration increased neuronal cFos expression in CaMKII-hM3Dq mice regardless of external input in both home-caged and fear-conditioned mice (*$p < 0.05$ for both).

(D and E) Representative images from mice expressing hM3Dq-mCherry (red) in their CA1 astrocytes (D) or neurons (E) that were injected with saline or CNO. Brain slices were stained for c-Fos (green) and the nuclear DAPI stain (blue) following either home-cage exposure or memory acquisition. cFos-expressing, activated astrocytes whose nuclei are out of the CA1 neuronal cell layers are clearly visible only in the GFAP-hM3Dq CNO-injected groups. Image frame colors correspond to group bars colors. Scale bar, 100 μm. Data are presented as mean ± SEM.

See also Figure S7.

CaMKII::hM3Dq mice increased neuronal cFos levels regardless of training, in both fear conditioned and home-caged mice (Figures 6C and 6E; $p < 0.05$ for both, t test). CNO alone had no effect on cFos levels in GFAP::eGFP mice in any condition (Figures S7A–S7C).

Our results show that astrocytic activation enhances neuronal activity in a task-dependent way, as demonstrated by its lack of effect on activity in home-caged mice, as opposed to the astrocyte-induced elevation in neuronal recruitment during memory allocation. Directly activating neurons, on the other hand, causes a non-selective increase in activity regardless of external experiences. This could explain why chemogenetic astrocytic activation improves memory, whereas neuronal activation impairs it.

Optogenetic Astrocytic Activation Improves Contextual Memory Acquisition

Our results show that chemogenetic astrocytic activation improves memory only when induced during acquisition, but not during recall. However, because CNO was administered 30 min before the task and remained in the body for several hours afterward, it could have affected not only memory acquisition but also early consolidation. To demonstrate the involvement of astrocytes specifically at the acquisition stage, we employed optogenetics, providing both cell-type specificity by confining expression to astrocytes and a strict temporal control by light administration, making it highly suitable for memory research (Fenno et al., 2011; Goshen, 2014).

Classical opsins, directly affecting the membrane potential, were used in the past to manipulate astrocytes in behaving mice (Gradinaru et al., 2009; Nam et al., 2016; Pelluru et al., 2016; Poskanzer and Yuste, 2016; Sasaki et al., 2012; Sweeney et al., 2016; Yamashita et al., 2014), though never in the hippocampus or in the cognitive tasks. It is not yet fully understood how such changes in membrane potential, which do not mimic any physiological processes, affect astrocytic function. Thus, we used the Opto-α1AR opsin, a light-sensitive Gq-coupled receptor (Airan et al., 2009), which is termed "OptoGq," to manipulate the Gq pathway in astrocytes in real time. This opsin was shown to specifically recruit the inositol triphosphate (IP_3) pathway and induce the release of Ca^{2+} from intracellular storage in HEK cells and in astrocytes (Airan et al., 2009; Figueiredo et al., 2014). We have produced an AAV viral vector to express OptoGq fused to eYFP under the GFAP promoter (AAV1-GFAP::OptoGq-eYFP) and delivered it to the CA1. OptoGq expression was limited to the astrocytic outer membrane (Figure 7A), with high penetrance (>87% of the GFAP cells expressed OptoGq) (Figure 1B) and almost complete specificity (>98% OptoGq-positive cells were also GFAP positive) (Figure 1C). To verify that optogenetic astrocytic activation does not have a direct effect on exploratory behavior that may alter freezing, we tested GFAP::OptoGq mice in an open field and found no effect of light administration (473 nm, 20 Hz, 45-ms pulse duration) on

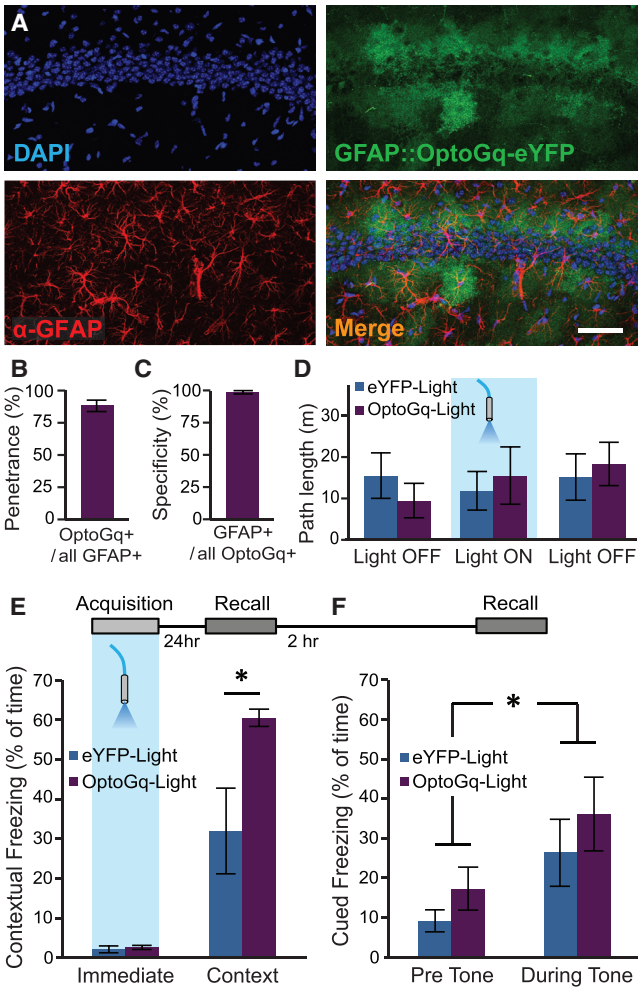

Figure 7. Optogenetic Astrocytic Activation Improves Contextual Memory Acquisition

(A) Bilateral double injection of AAV1-GFAP::OptoGq-eYFP resulted in OptoGq expression in CA1 astrocytes only: OptoGq (green) was expressed in the astrocytic membrane around the soma and in the distal processes (scale bar, 50 μm).

(B and C) GFAP::OptoGq was expressed in 87.4% of CA1 astrocytes (58/65 cells from 2 mice) (B), with 98.7% specificity (57/58 cells, from 2 mice) (C).

(D) Optogenetic activation of CA1 astrocytes had no effect on exploration of a novel environment, because eYFP control (n = 5) and GFAP-OptoGq (n = 5) mice explored the field with similar path lengths before, during, and after light administration.

(E) Optogenetic activation of CA1 astrocytes during fear-conditioning training had no effect on immediate freezing at the time of illumination, but increased contextual freezing by 89% (*p < 0.05) on the next day in GFAP::OptoGq (n = 5) mice compared to eYFP (n = 5) controls.

(F) Optogenetic activation of CA1 astrocytes during training had no effect on the acquisition of the hippocampal-independent auditory-cued fear memory in OptGq mice compared to controls, with both groups showing increased freezing during tone presentation (*p < 0.01). Data are presented as mean ± SEM.

exploration (Figure 7D). To specifically test the effect of astrocytic activation on fear memory acquisition, we administered light only during the 5-min training session. No real-time effect of light on immediate freezing following shock administration was observed (Figure 7E). Remarkably, light administration during training resulted in 89% elevation in contextual freezing in GFAP::OptoGq mice tested a day later (Figure 7E) ($p < 0.05$, t test). No effect on auditory-cued memory in a novel context was observed, i.e., both groups demonstrated similar freezing in response to the tone (Figure 7F) ($F_{(1,8)} = 11.19$, time main effect $p < 0.01$). To conclude, we show that real-time optogenetic astrocytic activation only during conditioning enhances memory acquisition, as demonstrated by improved recall a day later.

DISCUSSION

In recent years, it has become clear that astrocytes play an important role in neuronal activity and plasticity. In this work, we used advanced tools to specifically manipulate hippocampal astrocytes, and show for the first time that astrocytic activation can dramatically potentiate synaptic transmission, promote memory allocation, and improve memory performance. Specifically, even in the absence of any direct potentiating protocol delivered to the neurons, chemogenetic astrocytic activation generated *de novo*, sustainable, NMDA-dependent potentiation of CA3 to CA1 synapses. *In vivo*, astrocytic activation increased neuronal activity in a task-dependent manner only in learning mice, and enhanced cognitive performance in two memory tests. Finally, we show that optogenetic astrocytic activation precisely during memory acquisition induced a drastic memory enhancement.

The role of astrocytes in cognitive function is highly debated. Many studies demonstrated the necessity of astrocytes in memory, by showing that interrupting their activity leads to memory impairment (Gao et al., 2016; Gibbs et al., 2006; Halassa et al., 2009; Hertz and Gibbs, 2009; Newman et al., 2011; Stehberg et al., 2012; Suzuki et al., 2011; Tadi et al., 2015), and that correcting their genotype can alleviate memory impairments in genetic models of deficient cognition (Ben Menachem-Zidon et al., 2011; Han et al., 2012; Lioy et al., 2011). Interestingly, engraftment of human astrocytes to the brain of immune-deficient mice resulted in improved memory in these cognitively impaired animals (Han et al., 2013). On the other hand, other studies suggest that at least some astrocytic intracellular pathways are detrimental to memory function (Gerlai et al., 1995; Nishiyama et al., 2002; Orr et al., 2015). The combined picture arising from these seemingly contradicting results is that an optimal level of astrocytic activity is necessary to support intact memory, whereas excessive or deficient activity is harmful. Our behavioral results show that activating astrocytes by chemogenetic or optogenetic recruitment of their Gq-coupled signaling can bring them closer to this optimum, resulting in enhanced memory in both the T-maze and the FC tasks.

Conversely, we show that directly increasing the activity of CA1 neurons dramatically impairs memory acquisition. This finding is in agreement with optogenetic studies showing that unselective activation of dorsal DG or prefrontal cortex neurons during FC acquisition compromises recall on the next day (Kheirbek et al., 2013; Yizhar et al., 2011). However, pre-training neuronal activation is not necessarily detrimental. For example, when the activity of a small, selective neuronal population in

the BLA is increased before FC acquisition, a beneficial effect is conferred (Han et al., 2007; Yiu et al., 2014). Neurons active before training are also more likely to be allocated to the engram supporting the acquired memory (Josselyn et al., 2015).

Why then, does broad non-selective astrocytic activation enhance memory, whereas similar neuronal activation impairs it? Our results show a tailored response of astrocytes to the activity of their surrounding neurons, resulting in task-specific increase in neuronal activity, only in the ensemble active during memory allocation. Contrary to the non-selective increase in activity following chemogenetic stimulation of neurons, astrocytic activation does not increase baseline neuronal activity in the absence of an additional salient stimulus.

This selective effect of astrocytes brings to mind state of the art genetic tools that now offer activity-dependent neuronal targeting, allowing the specific tagging and manipulation of ensembles that were active during a specific time window (Allen et al., 2017; Liu et al., 2012; Ye et al., 2016). Like these tools, astrocytes, monitoring both the input and output information in their surrounding neuronal network, can detect and specifically enhance neuronal activity in response to a meaningful stimulus (such as SC stimulation in slice or FC *in vivo*), thus providing a similar activity-dependent specificity. This could explain why astrocytic activation improves memory performance, whereas neuronal activation impairs it.

To summarize, memory performance is not a simple binary process (remember/not remember), but can vary greatly both between and within memories. Memory ensemble allocation and maintenance depend on the activity level of neurons (Josselyn et al., 2015; Rogerson et al., 2014), which may well be contingent on their environment. As biological processes do not always reach their potential maxima, it is tempting to devise ways to enhance normal memory performance (Lee and Silva, 2009). Here, we show that activating astrocytes in mice with intact cognition improves their memory acquisition. In light of the justified hesitance to directly increase general neuronal activity, our finding that astrocytic modulation can enhance memory acquisition without affecting basal neuronal activity may have important clinical implications for cognitive augmentation treatments. The major advantage of using astrocytic modulation for this purpose is that the specificity of the effect is conferred by the astrocytes, not by the method of external manipulation, allowing straightforward translation to pharmacology.

Importantly, the capacity of astrocytes to independently induce plasticity and improve cognitive performance, as reported here, suggests that astrocytes can autonomously compute task-specific information based on the surrounding neuronal activity, which they then communicate back to the neuronal circuit. This perspective calls for a reassessment of the view of neuro-glia interaction, expanding the limited role of astrocytes as support cells merely enabling plastic and cognitive processes, to a broader function of these cells in actively shaping neuronal networks.

STAR★METHODS

Detailed methods are provided in the online version of this paper and include the following:

- KEY RESOURCES TABLE
- CONTACT FOR REAGENT AND RESOURCE SHARING
- EXPERIMENTAL MODEL AND SUBJECT DETAILS
  - Mice
- METHOD DETAILS
  - Stereotactic virus injection
  - Immunohistochemistry
  - Confocal Microscopy
  - Solutions for slice physiology
  - Behavioral testing
  - Virus production
- QUANTIFICATION AND STATISTICAL ANALYSIS
- DATA AND SOFTWARE AVAILABILITY

SUPPLEMENTAL INFORMATION

Supplemental Information includes seven figures can be found with this article online at https://doi.org/10.1016/j.cell.2018.05.002.

ACKNOWLEDGMENTS

We thank the entire Goshen lab for their support. We thank Karl Deisseroth (Stanford University) for the original OptoGq construct. We thank Ami Citri, Yaniv Ziv, Ofer Yizhar, and Raz Yirmiya for critically reading the manuscript. A.A., A.K., and A.D. were supported by an ELSC graduate students scholarship. A.D. was supported by the Azrieli Fellowship. T.K. was supported by an ELSC postdoc scholarship. I.G. was supported by the Israeli Centers of Research Excellence Program (center no. 1916/12), the Israel Science Foundation (ISF) (grant no. 1946/13), the NARSAD Young Investigator grant, the Abisch-Frenkel Foundation, the Alon Fellowship, and the Milton-Rosenbaum Foundation. M.L. is a Sachs Family Lecturer in Brain Science and is supported by the ISF, the Einstein Foundation, and the National Institute for Psychobiology.

AUTHOR CONTRIBUTIONS

A.A. contributed to behavioral and histology experiments; A.K. performed all slice electrophysiology; A.K. and A.D. performed Ca^{2+} imaging; T.K., T.M., R.R., and L.R. contributed to behavior and histology; N.O.-E. designed and built the slice electrophysiology setup; H.H. performed cloning; and M.G. produced the AAV for optogenetic manipulation. M.L. co-supervised slice electrophysiology and Ca^{2+} imaging. I.G. conceived of and supervised all aspects of the project and wrote the manuscript with assistance from M.L., A.A., and A.K.

DECLARATION OF INTERESTS

The authors declare no competing interests.

Received: October 11, 2017
Revised: January 31, 2018
Accepted: April 27, 2018
Published: May 24, 2018

REFERENCES

Adamsky, A., and Goshen, I. (2017). Astrocytes in memory function: pioneering findings and future directions. Neuroscience *370*, 14–26.

Agulhon, C., Petravicz, J., McMullen, A.B., Sweger, E.J., Minton, S.K., Taves, S.R., Casper, K.B., Fiacco, T.A., and McCarthy, K.D. (2008). What is the role of astrocyte calcium in neurophysiology? Neuron *59*, 932–946.

Agulhon, C., Boyt, K.M., Xie, A.X., Friocourt, F., Roth, B.L., and McCarthy, K.D. (2013). Modulation of the autonomic nervous system and behaviour by acute glial cell Gq protein-coupled receptor activation in vivo. J. Physiol. *591*, 5599–5609.

Airan, R.D., Thompson, K.R., Fenno, L.E., Bernstein, H., and Deisseroth, K. (2009). Temporally precise in vivo control of intracellular signalling. Nature *458*, 1025–1029.

Alexander, G.M., Rogan, S.C., Abbas, A.I., Armbruster, B.N., Pei, Y., Allen, J.A., Nonneman, R.J., Hartmann, J., Moy, S.S., Nicolelis, M.A., et al. (2009). Remote control of neuronal activity in transgenic mice expressing evolved G protein-coupled receptors. Neuron *63*, 27–39.

Allen, W.E., DeNardo, L.A., Chen, M.Z., Liu, C.D., Loh, K.M., Fenno, L.E., Ramakrishnan, C., Deisseroth, K., and Luo, L. (2017). Thirst-associated preoptic neurons encode an aversive motivational drive. Science *357*, 1149–1155.

Araque, A., Sanzgiri, R.P., Parpura, V., and Haydon, P.G. (1998). Calcium elevation in astrocytes causes an NMDA receptor-dependent increase in the frequency of miniature synaptic currents in cultured hippocampal neurons. J. Neurosci. *18*, 6822–6829.

Araque, A., Parpura, V., Sanzgiri, R.P., and Haydon, P.G. (1999). Tripartite synapses: glia, the unacknowledged partner. Trends Neurosci. *22*, 208–215.

Araque, A., Carmignoto, G., Haydon, P.G., Oliet, S.H., Robitaille, R., and Volterra, A. (2014). Gliotransmitters travel in time and space. Neuron *81*, 728–739.

Bazargani, N., and Attwell, D. (2016). Astrocyte calcium signaling: the third wave. Nat. Neurosci. *19*, 182–189.

Ben Menachem-Zidon, O., Avital, A., Ben-Menahem, Y., Goshen, I., Kreisel, T., Shmueli, E.M., Segal, M., Ben Hur, T., and Yirmiya, R. (2011). Astrocytes support hippocampal-dependent memory and long-term potentiation via interleukin-1 signaling. Brain Behav. Immun. *25*, 1008–1016.

Bonder, D.E., and McCarthy, K.D. (2014). Astrocytic Gq-GPCR-linked IP3R-dependent Ca2+ signaling does not mediate neurovascular coupling in mouse visual cortex in vivo. J. Neurosci. *34*, 13139–13150.

Bull, C., Freitas, K.C., Zou, S., Poland, R.S., Syed, W.A., Urban, D.J., Minter, S.C., Shelton, K.L., Hauser, K.F., Negus, S.S., et al. (2014). Rat nucleus accumbens core astrocytes modulate reward and the motivation to self-administer ethanol after abstinence. Neuropsychopharmacology *39*, 2835–2845.

Chai, H., Diaz-Castro, B., Shigetomi, E., Monte, E., Octeau, J.C., Yu, X., Cohn, W., Rajendran, P.S., Vondriska, T.M., Whitelegge, J.P., et al. (2017). Neural circuit-specialized astrocytes: transcriptomic, proteomic, morphological, and functional evidence. Neuron *95*, 531–549.e9.

Chen, N., Sugihara, H., Sharma, J., Perea, G., Petravicz, J., Le, C., and Sur, M. (2012). Nucleus basalis-enabled stimulus-specific plasticity in the visual cortex is mediated by astrocytes. Proc. Natl. Acad. Sci. USA *109*, E2832–E2841.

Chen, N., Sugihara, H., Kim, J., Fu, Z., Barak, B., Sur, M., Feng, G., and Han, W. (2016). Direct modulation of GFAP-expressing glia in the arcuate nucleus bi-directionally regulates feeding. eLife *5*, 5.

Dallérac, G., and Rouach, N. (2016). Astrocytes as new targets to improve cognitive functions. Prog. Neurobiol. *144*, 48–67.

Fenno, L., Yizhar, O., and Deisseroth, K. (2011). The development and application of optogenetics. Annu. Rev. Neurosci. *34*, 389–412.

Figueiredo, M., Lane, S., Stout, R.F., Jr., Liu, B., Parpura, V., Teschemacher, A.G., and Kasparov, S. (2014). Comparative analysis of optogenetic actuators in cultured astrocytes. Cell Calcium *56*, 208–214.

Frankland, P.W., and Bontempi, B. (2005). The organization of recent and remote memories. Nat. Rev. Neurosci. *6*, 119–130.

Gao, V., Suzuki, A., Magistretti, P.J., Lengacher, S., Pollonini, G., Steinman, M.Q., and Alberini, C.M. (2016). Astrocytic β2-adrenergic receptors mediate hippocampal long-term memory consolidation. Proc. Natl. Acad. Sci. USA *113*, 8526–8531.

Gerlai, R., Wojtowicz, J.M., Marks, A., and Roder, J. (1995). Overexpression of a calcium-binding protein, S100 beta, in astrocytes alters synaptic plasticity and impairs spatial learning in transgenic mice. Learn. Mem. *2*, 26–39.

Gibbs, M.E., Anderson, D.G., and Hertz, L. (2006). Inhibition of glycogenolysis in astrocytes interrupts memory consolidation in young chickens. Glia *54*, 214–222.

Goshen, I. (2014). The optogenetic revolution in memory research. Trends Neurosci. *37*, 511–522.

Gradinaru, V., Mogri, M., Thompson, K.R., Henderson, J.M., and Deisseroth, K. (2009). Optical deconstruction of parkinsonian neural circuitry. Science *324*, 354–359.

Halassa, M.M., Florian, C., Fellin, T., Munoz, J.R., Lee, S.Y., Abel, T., Haydon, P.G., and Frank, M.G. (2009). Astrocytic modulation of sleep homeostasis and cognitive consequences of sleep loss. Neuron *61*, 213–219.

Han, J.H., Kushner, S.A., Yiu, A.P., Cole, C.J., Matynia, A., Brown, R.A., Neve, R.L., Guzowski, J.F., Silva, A.J., and Josselyn, S.A. (2007). Neuronal competition and selection during memory formation. Science *316*, 457–460.

Han, J., Kesner, P., Metna-Laurent, M., Duan, T., Xu, L., Georges, F., Koehl, M., Abrous, D.N., Mendizabal-Zubiaga, J., Grandes, P., et al. (2012). Acute cannabinoids impair working memory through astroglial CB1 receptor modulation of hippocampal LTD. Cell *148*, 1039–1050.

Han, X., Chen, M., Wang, F., Windrem, M., Wang, S., Shanz, S., Xu, Q., Oberheim, N.A., Bekar, L., Betstadt, S., et al. (2013). Forebrain engraftment by human glial progenitor cells enhances synaptic plasticity and learning in adult mice. Cell Stem Cell *12*, 342–353.

Haydon, P.G. (2001). GLIA: listening and talking to the synapse. Nat. Rev. Neurosci. *2*, 185–193.

Henneberger, C., Papouin, T., Oliet, S.H., and Rusakov, D.A. (2010). Long-term potentiation depends on release of D-serine from astrocytes. Nature *463*, 232–236.

Hertz, L., and Gibbs, M.E. (2009). What learning in day-old chickens can teach a neurochemist: focus on astrocyte metabolism. J. Neurochem. *109* (*Suppl 1*), 10–16.

Josselyn, S.A., Köhler, S., and Frankland, P.W. (2015). Finding the engram. Nat. Rev. Neurosci. *16*, 521–534.

Jourdain, P., Bergersen, L.H., Bhaukaurally, K., Bezzi, P., Santello, M., Domercq, M., Matute, C., Tonello, F., Gundersen, V., and Volterra, A. (2007). Glutamate exocytosis from astrocytes controls synaptic strength. Nat. Neurosci. *10*, 331–339.

Kheirbek, M.A., Drew, L.J., Burghardt, N.S., Costantini, D.O., Tannenholz, L., Ahmari, S.E., Zeng, H., Fenton, A.A., and Hen, R. (2013). Differential control of learning and anxiety along the dorsoventral axis of the dentate gyrus. Neuron *77*, 955–968.

Lee, Y.S., and Silva, A.J. (2009). The molecular and cellular biology of enhanced cognition. Nat. Rev. Neurosci. *10*, 126–140.

Lioy, D.T., Garg, S.K., Monaghan, C.E., Raber, J., Foust, K.D., Kaspar, B.K., Hirrlinger, P.G., Kirchhoff, F., Bissonnette, J.M., Ballas, N., and Mandel, G. (2011). A role for glia in the progression of Rett's syndrome. Nature *475*, 497–500.

Liu, X., Ramirez, S., Pang, P.T., Puryear, C.B., Govindarajan, A., Deisseroth, K., and Tonegawa, S. (2012). Optogenetic stimulation of a hippocampal engram activates fear memory recall. Nature *484*, 381–385.

López, A.J., Kramár, E., Matheos, D.P., White, A.O., Kwapis, J., Vogel-Ciernia, A., Sakata, K., Espinoza, M., and Wood, M.A. (2016). Promoter-specific effects of DREADD modulation on hippocampal synaptic plasticity and memory formation. J. Neurosci. *36*, 3588–3599.

Martin-Fernandez, M., Jamison, S., Robin, L.M., Zhao, Z., Martin, E.D., Aguilar, J., Benneyworth, M.A., Marsicano, G., and Araque, A. (2017). Synapse-specific astrocyte gating of amygdala-related behavior. Nat. Neurosci. *20*, 1540–1548.

Min, R., and Nevian, T. (2012). Astrocyte signaling controls spike timing-dependent depression at neocortical synapses. Nat. Neurosci. *15*, 746–753.

Nam, Y., Kim, J.H., Kim, J.H., Jha, M.K., Jung, J.Y., Lee, M.G., Choi, I.S., Jang, I.S., Lim, D.G., Hwang, S.H., et al. (2016). Reversible induction of pain hypersensitivity following optogenetic stimulation of spinal astrocytes. Cell Rep. *17*, 3049–3061.

Navarrete, M., Perea, G., Fernandez de Sevilla, D., Gómez-Gonzalo, M., Núñez, A., Martín, E.D., and Araque, A. (2012). Astrocytes mediate in vivo cholinergic-induced synaptic plasticity. PLoS Biol. *10*, e1001259.

Newman, L.A., Korol, D.L., and Gold, P.E. (2011). Lactate produced by glycogenolysis in astrocytes regulates memory processing. PLoS ONE *6*, e28427.

Nishiyama, H., Knopfel, T., Endo, S., and Itohara, S. (2002). Glial protein S100B modulates long-term neuronal synaptic plasticity. Proc. Natl. Acad. Sci. USA *99*, 4037–4042.

Oliveira, J.F., Sardinha, V.M., Guerra-Gomes, S., Araque, A., and Sousa, N. (2015). Do stars govern our actions? Astrocyte involvement in rodent behavior. Trends Neurosci. *38*, 535–549.

Orr, A.G., Hsiao, E.C., Wang, M.M., Ho, K., Kim, D.H., Wang, X., Guo, W., Kang, J., Yu, G.Q., Adame, A., et al. (2015). Astrocytic adenosine receptor A2A and Gs-coupled signaling regulate memory. Nat. Neurosci. *18*, 423–434.

Panatier, A., Vallée, J., Haber, M., Murai, K.K., Lacaille, J.C., and Robitaille, R. (2011). Astrocytes are endogenous regulators of basal transmission at central synapses. Cell *146*, 785–798.

Pascual, O., Casper, K.B., Kubera, C., Zhang, J., Revilla-Sanchez, R., Sul, J.Y., Takano, H., Moss, S.J., McCarthy, K., and Haydon, P.G. (2005). Astrocytic purinergic signaling coordinates synaptic networks. Science *310*, 113–116.

Pelluru, D., Konadhode, R.R., Bhat, N.R., and Shiromani, P.J. (2016). Optogenetic stimulation of astrocytes in the posterior hypothalamus increases sleep at night in C57BL/6J mice. Eur. J. Neurosci. *43*, 1298–1306.

Perea, G., and Araque, A. (2007). Astrocytes potentiate transmitter release at single hippocampal synapses. Science *317*, 1083–1086.

Poskanzer, K.E., and Yuste, R. (2016). Astrocytes regulate cortical state switching in vivo. Proc. Natl. Acad. Sci. USA *113*, E2675–E2684.

Rogerson, T., Cai, D.J., Frank, A., Sano, Y., Shobe, J., Lopez-Aranda, M.F., and Silva, A.J. (2014). Synaptic tagging during memory allocation. Nat. Rev. Neurosci. *15*, 157–169.

Roth, B.L. (2016). DREADDs for neuroscientists. Neuron *89*, 683–694.

Santello, M., Bezzi, P., and Volterra, A. (2011). TNFα controls glutamatergic gliotransmission in the hippocampal dentate gyrus. Neuron *69*, 988–1001.

Sasaki, T., Beppu, K., Tanaka, K.F., Fukazawa, Y., Shigemoto, R., and Matsui, K. (2012). Application of an optogenetic byway for perturbing neuronal activity via glial photostimulation. Proc. Natl. Acad. Sci. USA *109*, 20720–20725.

Scofield, M.D., Boger, H.A., Smith, R.J., Li, H., Haydon, P.G., and Kalivas, P.W. (2015). Gq-DREADD selectively initiates glial glutamate release and inhibits cue-induced cocaine seeking. Biol. Psychiatry *78*, 441–451.

Shigetomi, E., Bushong, E.A., Haustein, M.D., Tong, X., Jackson-Weaver, O., Kracun, S., Xu, J., Sofroniew, M.V., Ellisman, M.H., and Khakh, B.S. (2013). Imaging calcium microdomains within entire astrocyte territories and endfeet with GCaMPs expressed using adeno-associated viruses. J. Gen. Physiol. *141*, 633–647.

Stehberg, J., Moraga-Amaro, R., Salazar, C., Becerra, A., Echeverría, C., Orellana, J.A., Bultynck, G., Ponsaerts, R., Leybaert, L., Simon, F., et al. (2012). Release of gliotransmitters through astroglial connexin 43 hemichannels is necessary for fear memory consolidation in the basolateral amygdala. FASEB J. *26*, 3649–3657.

Suzuki, A., Stern, S.A., Bozdagi, O., Huntley, G.W., Walker, R.H., Magistretti, P.J., and Alberini, C.M. (2011). Astrocyte-neuron lactate transport is required for long-term memory formation. Cell *144*, 810–823.

Sweeney, P., Qi, Y., Xu, Z., and Yang, Y. (2016). Activation of hypothalamic astrocytes suppresses feeding without altering emotional states. Glia *64*, 2263–2273.

Tadi, M., Allaman, I., Lengacher, S., Grenningloh, G., and Magistretti, P.J. (2015). Learning-induced gene expression in the hippocampus reveals a role of neuron-astrocyte metabolic coupling in long term memory. PLoS ONE *10*, e0141568.

Takata, N., Mishima, T., Hisatsune, C., Nagai, T., Ebisui, E., Mikoshiba, K., and Hirase, H. (2011). Astrocyte calcium signaling transforms cholinergic modulation to cortical plasticity in vivo. J. Neurosci. *31*, 18155–18165.

Tanaka, K.Z., Pevzner, A., Hamidi, A.B., Nakazawa, Y., Graham, J., and Wiltgen, B.J. (2014). Cortical representations are reinstated by the hippocampus during memory retrieval. Neuron *84*, 347–354.

Whitlock, J.R., Heynen, A.J., Shuler, M.G., and Bear, M.F. (2006). Learning induces long-term potentiation in the hippocampus. Science *313*, 1093–1097.

Yamashita, A., Hamada, A., Suhara, Y., Kawabe, R., Yanase, M., Kuzumaki, N., Narita, M., Matsui, R., Okano, H., and Narita, M. (2014). Astrocytic activation in the anterior cingulate cortex is critical for sleep disorder under neuropathic pain. Synapse *68*, 235–247.

Yang, L., Qi, Y., and Yang, Y. (2015). Astrocytes control food intake by inhibiting AGRP neuron activity via adenosine A1 receptors. Cell Rep. *11*, 798–807.

Ye, L., Allen, W.E., Thompson, K.R., Tian, Q., Hsueh, B., Ramakrishnan, C., Wang, A.C., Jennings, J.H., Adhikari, A., Halpern, C.H., et al. (2016). Wiring and molecular features of prefrontal ensembles representing distinct experiences. Cell *165*, 1776–1788.

Yiu, A.P., Mercaldo, V., Yan, C., Richards, B., Rashid, A.J., Hsiang, H.L., Pressey, J., Mahadevan, V., Tran, M.M., Kushner, S.A., et al. (2014). Neurons are recruited to a memory trace based on relative neuronal excitability immediately before training. Neuron *83*, 722–735.

Yizhar, O., Fenno, L.E., Prigge, M., Schneider, F., Davidson, T.J., O'Shea, D.J., Sohal, V.S., Goshen, I., Finkelstein, J., Paz, J.T., et al. (2011). Neocortical excitation/inhibition balance in information processing and social dysfunction. Nature *477*, 171–178.

STAR★METHODS

KEY RESOURCES TABLE

REAGENT or RESOURCE	SOURCE	IDENTIFIER
Antibodies		
Chicken anti-GFAP	Millipore	Cat#AB5541; RRID:AB_177521
Rabbit anti-Iba1	Wako	Cat#019-19471; RRID:AB_2665520
Rabbit anti-NeuN	Cell Signaling Technology	Cat#12943; RRID:AB_2630395
Goat anti-mCherry	LifeSpan	Cat#LS-C204207; RRID:AB_2619713
Rabbit anti c-fos	Synaptic Systems	Cat#226 003; RRID:AB_2231974
Donkey anti-chicken (Alexa Fluor 488)	Jackson ImmunoResearch Labs	Cat#703-545-155; RRID:AB_2340375
Donkey anti-rabbit (Alexa Fluor 488)	Jackson ImmunoResearch Labs	Cat#711-545-152; RRID:AB_2313584
Donkey anti-goat (Alexa Fluor 594)	Jackson ImmunoResearch Labs	Cat#705-585-003; RRID:AB_2340432
Bacterial and Virus Strains		
AAV8-GFAP-hM3D(Gq)-mCherry	UNC vector core	N/A
AAV8-GFAP-mCherry	UNC vector core	N/A
AAV8-GFAP-eGFP	UNC vector core	N/A
AAV8-CaMKIIa-hM3D(Gq)-mCherry	AddGene	Cat#50476
AAV5-GfaABC1D-cytoGCaMP6f-sv40	UPenn vector core	Cat#AV-5-52925
AAV1-GfaABC1D-OptoGq-eYFP	ELSC Vector Core Facility	N/A
Chemicals, Peptides, and Recombinant Proteins		
Alexafluor 594	Life Technologies	Cat#A10438
Alexafluor 488	Life Technologies	Cat#A10436
Tetrodotoxin (TTX)	Alomone Labs	Cat#T-550
D-(-)-2-Amino-5-phosphonopentanoic acid (D-AP5)	Tocris Bioscience	Cat#0106; CAS: 79055-68-8
D-Serine	Tocris Bioscience	Cat#0226; CAS: 312-84-5
5,7-Dichlorokynurenic acid (DCKA)	Tocris Bioscience	Cat#0286; CAS: 131123-76-7
2-Methyl-6-(phenylethynyl)pyridine (MPEP)	Tocris Bioscience	Cat#1212; CAS: 219911-35-0
(*S*)-(+)-α-Amino-4-carboxy-2-methylbenzeneacetic acid (LY367385)	Tocris Bioscience	Cat#1237; CAS: 198419-91-9
Ethylene glycol-bis(2-aminoethylether)-N,N,N′,N′-tetraacetic acid (EGTA)	Sigma	Cat#E3889; CAS: 67-42-5
Clozapine *N*-oxide (CNO)	Tocris Bioscience	Cat#4936; CAS: 34233-69-7
Neurobiotin 488	Vector Labs	Cat#SP-1125
Deposited Data		
Raw data	https://data.mendeley.com/datasets/9dnftn9856/draft?a=1df3cf22-5e00-4ed1-b251-83e5e0d152f6	N/A
Experimental Models: Organisms/Strains		
C57BL/6JOlaHsd	Harlan	N/A
Recombinant DNA		
AAV-GfaABC1D-OptoGq-eYFP	This paper	N/A
Software and Algorithms		
EthoVision tracking software version 13	Noldus	https://www.noldus.com/animal-behavior-research/products/ethovision-xt
pCLAMP version 10.6.2	Molecular Devices	http://mdc.custhelp.com/app/answers/detail/a_id/18779/~/axon%E2%84%A2-pclamp%E2%84%A2-10-electrophysiology-data-acquisition-%26-analysis-software

(*Continued on next page*)

Continued

REAGENT or RESOURCE	SOURCE	IDENTIFIER
MATLAB 2015	MathWorks	https://www.mathworks.com/products/matlab.html
IBM SPSS statistics version 24	IBM Analytics	https://www.ibm.com/analytics/data-science/predictive-analytics/spss-statistical-software
Olympus Fluoview Viewer version 4.2	Olympus	https://www.olympus-lifescience.com/en/support/downloads/
Bitplane IMARIS 7.6.3	Bitplane	http://www.bitplane.com/imaris?gclid=Cj0KCQiA2snUBRDfARIsAIGfpqHJaUyUtg02Tia374tZOGCSXW8IDrURqjtkTBv9y1aolCv9a-1pS04aArgXEALw_wcB
LotosScan	Suzhou Institute of Biomedical Engineering and Technology	http://english.sibet.cas.cn/
ImageJ	National Institutes of Health	https://imagej.nih.gov/ij/
Scanbox	Neurolabware	http://neurolabware.com/

CONTACT FOR REAGENT AND RESOURCE SHARING

Further information and requests for resources and reagents should be directed to and will be fulfilled by the Lead Contact, Inbal Goshen (inbal.goshen@elsc.huji.ac.il).

EXPERIMENTAL MODEL AND SUBJECT DETAILS

Mice

Male C57BL/6 mice, 6-7 weeks old (Harlan) were group housed on a 12 hr light/dark cycle with *ad libitum* access to food and water. All mice were maintained under pathogen-free conditions in Tecniplast cages, on Teklad sani-chips (ENVIGO) bedding, at 20-24°C, and fed Teklad 2918SC (ENVIGO) pellets. Mice were randomly assigned to experimental groups. Experimental protocols were approved by the Hebrew University Animal Care and Use Committee and met the guidelines of the National Institute of Health guide for the Care and Use of Laboratory Animals.

METHOD DETAILS

Stereotactic virus injection

Mice were anesthetized with isoflurane, and their head placed in a stereotactic apparatus (Kopf Instruments, USA). The skull was exposed and a small craniotomy was performed. To cover the entire dorsal CA1, mice were bilaterally microinjected in two sites per hemisphere using the following coordinates: site 1: anteroposterior (AP), −1.5mm from Bregma, mediolateral (ML), ± 1mm, dorsoventral (DV), −1.55mm; site 2: AP −2.5mm, ML ± 2mm, DV −1.55mm. All microinjections were carried out using a 10μl syringe and a 34 gauge metal needle (WPI, Sarasota, USA). The injection volume and flow rate (0.1 μl/min) were controlled by an injection pump (WPI). Following each injection, the needle was left in place for 10 additional minutes to allow for diffusion of the viral vector away from the needle track, and was then slowly withdrawn. For the optogenetic experiment, a bilateral patchcord (a dual metal ferrule 2.5 mm center to center; with a 300 μm thick, 3 mm long, cleaved bare optic fiber; Doric lenses Inc., Quebec, Canada) was then placed above CA1 (AP, −1.94 mm, ML, ± 1.25 mm, DV −1 mm), and secured to the skull using dental cement (C&B Metabond, Parkell, Edgwood, NY). The incision was closed using Vetbond tissue adhesive. For postoperative care, mice were subcutaneously injected with Tramadex (5mg/kg).

Viral vectors

AAV8-GFAP-hM3D(Gq)-mCherry, AAV8-GFAP-eGFP, AAV8-GFAP-mCherry (UNC vector core), and AAV1-GfaABC1D-OptoGq-eYFP (ELSC Vector Core Facility) were diluted 1:10 in PBS and injected with a volume of 700nl/site. AAV8-CaMKIIa-hM3D(Gq)-mCherry (AddGene) was injected with a volume of 500-700nl/site without dilution. AAV5-GfaABC1D-cytoGCaMP6f-sv40 (UPenn vector core) was injected with a volume of 800nl/site without dilution (see also Key Resources Table).

Immunohistochemistry

Three weeks post injection, mice were transcardially perfused with cold PBS followed by 4% paraformaldehyde (PFA) in PBS. The brains were extracted, postfixed overnight in 4% PFA at 4°C, and cryoprotected in 30% sucrose in PBS. Brains were sectioned to a thickness of 40 μm using a sliding freezing microtome (Leica SM 2010R) and preserved in a cryoprotectant solution (25% glycerol and

30% ethylene glycol, in PBS). Free-floating sections were washed in PBS, incubated for 1 hr in blocking solution (3% normal donkey serum (NDS) and 0.3% Triton X-100 in PBS), and incubated overnight at 4°C with primary antibodies (chicken anti-GFAP, Millipore, 1:500; rabbit anti-Iba1, Wako, 1:500; rabbit anti-NeuN, Cell Signaling Technology, 1:400; goat anti-mCherry, LifeSpan BioSciences, 1:200) in 0.1% Triton and 3% NDS in PBS. For the cFos staining, slices were incubated with the primary antibody (rabbit anti c-*fos*, Synaptic Systems, 1:10,000) for 5 nights at 4°C. Sections were then washed with PBS and incubated for 2 hr at room temperature with secondary antibodies (donkey anti-chicken, Alexa Fluor 488, 1:500; donkey anti-rabbit, Alexa Fluor 488, 1:500; donkey anti-goat, Alexa Fluor 594, 1:400) in 3% NDS in PBS. Finally, sections were washed in PBS, incubated with DAPI (1μg/ml), mounted on slides and sealed with mounting medium (Flouromount-G, eBioscience, San-Diego, CA, USA). mCherry was stained only for the 3D reconstruction in Figure 1G. See Key Resources Table for the catalog numbers and RRIDs of all antibodies.

Confocal Microscopy

Confocal fluorescence images were acquired on an Olympus scanning laser microscope Fluoview FV1000 using 4X and 10X air objectives or 20X and 40X oil immersion objectives. Image analysis was performed using the Olympus Fluoview Viewer version 4.2. 3D image was created by imaging 0.5 μm thick optical plains of 40 μm thick brain sections and then reconstructing them using Bitplane IMARIS 7.6.3 software.

Ca^{2+} imaging

Coronal hippocampal slices (300 μm) were made from 11-12 weeks old mice. Animals were anesthetized with isoflurane, and the brain was swiftly removed, mounted frontal-side up and sliced in ice-cold oxygenated low-Ca^{2+} ACSF (see below precise content) using a vibratome (Campden Instruments). Slices were then incubated for 1hr in a holding chamber with oxygenated normal Ca^{2+} ACSF at 35°C and then kept at 32°C. Individual slices were transferred to a submerged recording chamber (34°C), and astrocytes expressing both hM3Dq-mCherry and GCaMP6f were selected for imaging.

For the acute CNO application experiment, imaging was performed with a low-power temporal oversampling (LOTOS) two-photon microscope (LotosScan2015, Suzhou Institute of Biomedical Engineering and Technology, http://english.sibet.cas.cn/). mCherry and Alexa 594 were excited at 920nm, and GCaMP6f was excited at 920 nm, with a Ti:Sapphire laser (Vision II, Coherent Inc., CA) and imaged through a 25X, 1.05 NA water immersion objective (Olympus, Japan). Full frame images (600 × 600 pixels) were acquired at 40 frames/second. Image acquisition was performed using a LabView based software (LotosScan), and Images were analyzed with ImageJ (NIH) and MATLAB.

A glass pipette loaded with red fluorescent dye (Alexa 594) was visually guided and placed near a target astrocyte (Figure 1H). In addition the pipette solution contained either ACSF or ACSF with CNO (10mM). Application of a 20 PSI increase in pressure to the pipette for 200msec resulted in an increase of the spread of the red indicator (Figure 1I) and the fluorescence of the Ca^{2+} indicator was measured from 60sec before to 60sec after drug application.

For the prolonged CNO application experiment (Figure S1), 2-Photon imaging was performed using the Neurolabware 2-photon laser scanning microscope (Los Angeles, CA, USA). The microscope consists of a 6215 galvometer and a CRS8 resonant mirror (Cambridge Technology), and a water immersion 16X objective (Nikon, 0.8 NA). The Ti:sapphire excitation laser (Chameleon Vision II, Coherent) was operated at 920 nm and directed to a GaAsP PMT (H10770PA-40; Hamamatsu) through a series of mirrors and band pass filters (Semrock). XYZ motion control was obtained using motorized linear stages, enabled via an electronic rotary encoder (KnobbyII). Images were acquired at 15.5 frames/second. The Scanbox software, run on MATLAB, was used for microscope control and acquisition. The FIJI open source program was used for motion correction (MOCO plugin) and ROI selection and signal extraction. Signal processing and analysis was conducted using MATLAB. Astrocytes co-expressing GCaMP6f and mCherry were imaged under TTX (0.5 μM), to separate astrocytic activity from the neuronal one. First, astrocytes were imaged for 5 minutes to determine baseline Ca^{2+} activity. CNO or ACSF were then added to the chamber, and imaging was resumed after a 15 minutes break. Astrocytes were then imaged three times for 5 minutes separated by a 5 minutes interval. Finally, CNO was washed out of the chamber for 20 minutes, and astrocytes were imaged twice in 5 minute long trials separated by a 5 minute interval.

For data analysis ΔF/F was calculated as follows: $100 * (F_t - F_0)/F_0$, where F(t) is the mean florescent response of the ROI in each frame and F_0 is the mode of F(t) for the entire trial.

Slice Electrophysiology

Coronal hippocampal slices (350 μm) were made from 11-12 weeks old C57 mice. Animals were anesthetized with isoflurane, and their brains were swiftly removed, mounted frontal-side up and sliced in ice-cold oxygenated low Ca^{2+} ACSF (see below the precise content of all solutions) using a vibratome (Campden Instruments). Slices were then incubated for 1hr in a holding chamber with oxygenated normal Ca^{2+} ACSF at 35°C and then kept at 32°C. Individual slices were transferred to a submerged recording chamber (32°C), and somata selected for recordings based on their pyramidal shape. Patch electrodes were fabricated from fire polished thick walled borosilicate glass, and filled with internal solution (see below). Electrode resistance in the bath ranged 4-8 MΩ and series resistance ranged 12-35 MΩ.

In all voltage clamp experiments cells were held at resting potential of −70mV. Miniature EPSCs were recorded in the presence of TTX (1 μM; applied 10min before recording), for 5min either before or 15min after CNO (10 μM) bath application, and analyzed offline using MATLAB. The second recording was 15min after changing the bath perfusion solution, to allow full replacement of ACSF with ACSF+CNO solution (Figure 2B). The events were detected based on amplitude and 1st derivative, where the minimum amplitude was −3pA.

For synaptic stimulation a bipolar tungsten electrode (WPI Inc.) was placed on the Schaffer collaterals at least 200 μm away from the recording electrode. Single electrical stimulation was 0.2ms with strength ranging 50-140 μA, calibrated to induce 50% of maximal EPSC. EPSC recordings were performed for 10 minutes, either before or 15 minutes after CNO bath application (Figures 3A and 3B). Recordings were carried out using a Multiclamp 700B patch-clamp amplifier (Molecular Devices). Signals were low-pass filtered at 3 kHz, digitized and sampled through an AD converter (Molecular Devices) at 20kHz, and stored for offline analysis using MATLAB.

For extracellular field EPSP recordings, 400 μm coronal hippocampal slices were prepared, and stimuli to the Schaffer collaterals were administered as described above. fEPSPs were recorded in the CA1 stratum radiatum using a glass pipette containing ACSF (2-6MΩ). fEPSPs were low-pass filtered at 400 Hz, digitized and sampled through an AD converter at 10 kHz, and stored for offline analysis using MATLAB.

For the Ca^{2+} chelation experiment slices were prepared and data was extracted as above. Before field recording, an astrocyte was patched and filled with an internal solution containing EGTA, and $CaCl_2$ to clamp intracellular free Ca^{2+} at a steady-state concentration of 50–80 nM (calculated by WebMaxChelator). Internal solution composition: 10 Mm NaCl, 10 mM HEPES, 140mM k-gluconate, 0.5mM $MgCl_2$, 0.4mM Na_3GTP, 4mM MgATP, 0.14mM $CaCl_2$, 0.45 mM EGTA (Sigma). The pH of the internal solution was adjusted to 7.3 with KOH. Alexafluor488 (80 μM, Life Technologies) was added and the osmolarity was set to 285–290 mOsm. To verify that the patched cells are astrocytes, we injected step current in current clamp (steps of 100 pA from −500 pA to +500 pA) and step voltage in voltage clamp (5 mV steps, from −90 mV to +90 mV) and recorded typical non-excitable responses. The patch was held for 40 minutes, to allow diffusion of EGTA to a group of adjacent astrocytes, and then the pipette was removed and replaced by a field recording pipette positioned either adjacent to or distant from the patch site.

Solutions for slice physiology

Low-Ca^{2+}ACSF:

126 mM NaCl, 2.6 mM KCl, 26 mM $NaHCO_3$, 1.25 mM NaH_2PO_4, 10 mM Glucose, 1 mM $MgCl_2$, 0.625 mM $CaCl_2$.

Normal-Ca^{2+}ACSF:

126 mM NaCl, 2.6 mM KCl, 26 mM $NaHCO_3$, 1.25 mM NaH_2PO_4, 10 mM Glucose, 1 mM $MgCl_2$, 2 mM $CaCl_2$.

Normal-$Ca^{2+}$with 2mM Magnesium ACSF:

126 mM NaCl, 2.6 mM KCl, 26 mM $NaHCO_3$, 1.25 mM NaH_2PO_4, 10 mM Glucose, 2 mM $MgCl_2$, 2 mM $CaCl_2$.

The pH of the ACSF was set to 7.3 and the osmolarity to 305–320 mOsm. ACSF was oxygenated and pH buffered by constant bubbling with a gas mixture of 95% O2/5% CO2.

Internal solution

120 mM cesium methanesulfonate, 20 mM HEPES, 0.4 mM EGTA, 2.8 Mm NaCl, 5 mM TEA. The pH of the internal solution was set to 7.3–7.4 using 0.2 M CsOH. The osmolarity was set to 275–285 mOsm.

Behavioral testing

Experimental design

Mice from different experimental groups were randomly distributed in all cages, and experimenters were blind to their group allocation. All measurements were performed automatically, preventing any experimenter-induced bias. Experiment replication is specified in the result section.

T-maze

Training and testing were conducted in a T shaped elevated maze (30X10cm start arm and two 30X10cm goal arms, with stripes or circles on the walls of the goal arms). During training, one of the goal arms was blocked, mice were placed in the start arm facing away from the choice point, and allowed to freely explore the maze for 20 min. The retention test was performed 5 min after training. During this test both goal arms were open, mice were placed at the end of the start arm facing away from the choice point and allowed to freely explore for 5 min. The percent of time spent in each arm and the total exploration (in meters) were measured using the EthoVision tracking software (Noldus). New arm preference was calculated by dividing the percentage of time spent in the new arm (that was closed during training) by the percentage of time spent in both goal arms (new and old).

FC

The FC apparatus consisted of a conditioning box (18x18x30 cm), with a grid floor wired to a shock generator surrounded by an acoustic chamber (Ugo Basile), and controlled by the EthoVision software (Noldus). Three weeks after injections, mice were placed in the conditioning box for 2min, and then a pure tone (2.9 kHz) was sounded for 20sec, followed by a 2sec foot shock (0.4mA). This procedure was then repeated, and 30sec after the delivery of the second shock mice were returned to their home cages. FC was assessed by a continuous measurement of freezing (complete immobility), the dominant behavioral fear response. Freezing was automatically measured throughout the testing trial by the EthoVision tracking software. To test contextual FC, mice were placed in the original conditioning box, and freezing was measured for 5min. To test auditory-cued FC, mice were placed in a different context (a cylinder-shaped cage with stripes on the walls and a smooth floor), freezing was measured for 2.5min, and then a 2.9kHz tone was sounded for 2.5min, during which conditioned freezing was measured.

Open Field

The OF test was conducted in a round plastic arena, 54 cm in diameter. Mice were placed in the center of the arena and allowed to freely explore it for 5min. Total exploration distance (in meters) and percent time spent in the central 35% of the arena were measured using the EthoVision tracking software.

CNO administration

CNO was dissolved in DMSO and then diluted in 0.9% saline to yield a final DMSO concentration of 0.5%. Saline solution for control injections also consisted of 0.5% DMSO. 3mg/kg CNO was intraperitoneally injected 30min before the behavioral assays. The chosen doses of CNO did not induce any behavioral signs of seizure activity. For the second neuronal activation experiment (Figure S6) a lower dose of 0.5mg/kg was used.

Light administration

To optogenetically activate astrocytes, blue light (473 nm, Laserglow Technologies, Toronto, Canada) was bilaterally delivered through two 300μm thick optic fibers ending in a metal ferrule (Doric lenses) that were attached to the transplanted patchcords by connecting plastic sleeves. Light was delivered throughout the five minutes of fear-conditioning training, in a 90% duty cycle (20Hz, pulse duration 45msec). In the open field test the mice explored the field for 3 minutes with no light (Light OFF). Light was then delivered for 3 minutes (Light ON), and turned off (Light OFF) for the last 3 minutes of the test.

Virus production

The adeno-associated virus (AAV) AAV-GfaABC1D-OptoGq-eYFP plasmid was constructed by cloning the gfaABC1D promoter (Shigetomi et al., 2013) into an AAV backbone. pZac2.1 gfaABC1D-tdTomato was a gift from Prof. Baljit Khakh (Addgene plasmid # 44332). Subsequently, OptoGq-eYFP (a gift from Prof. Karl Deisseroth, Stanford University) was inserted into this backbone using the AgeI and EcoRI restriction sites. The recombinant AAV vectors were serotyped with AAV1 coat proteins and packaged by the ELSC Vector Core Facility at the Hebrew University of Jerusalem.

QUANTIFICATION AND STATISTICAL ANALYSIS

Data is presented as mean ± standard error of the mean (SEM) unless otherwise indicated in figure legends. Sample number (n) indicates the number of cells or mice in each experiment and is specified in the figure legends. When the data met the assumptions of parametric statistical tests, results were analyzed by Student's t test or two-way ANOVA, followed by LSD post hoc tests, as applicable. Data was tested for normality by using the Shapiro-Wilk test of normality, and for homogeneity of variances by using the Levene's test for homogeneity of variances. For longitudinal data with missing observation, a linear mixed model was used to analyze the results, followed by pairwise comparisons with Sidak adjustment for multiple comparisons. When the data did not meet the assumptions of parametric statistical tests two sample Kolmogorov-Smirnov test was used to compare two probability distributions. All the statistical details of experiments can be found in the result section. Differences in means were considered statistically significant at $p < 0.05$. Analyses were performed using the IBM SPSS Statistics software (version 24). Subjects were excluded from analysis when they deviated by more than two standard deviations from the mean.

DATA AND SOFTWARE AVAILABILITY

All data is available at: https://data.mendeley.com/datasets/9dnftn9856/draft?a=1df3cf22-5e00-4ed1-b251-83e5e0d152f6.

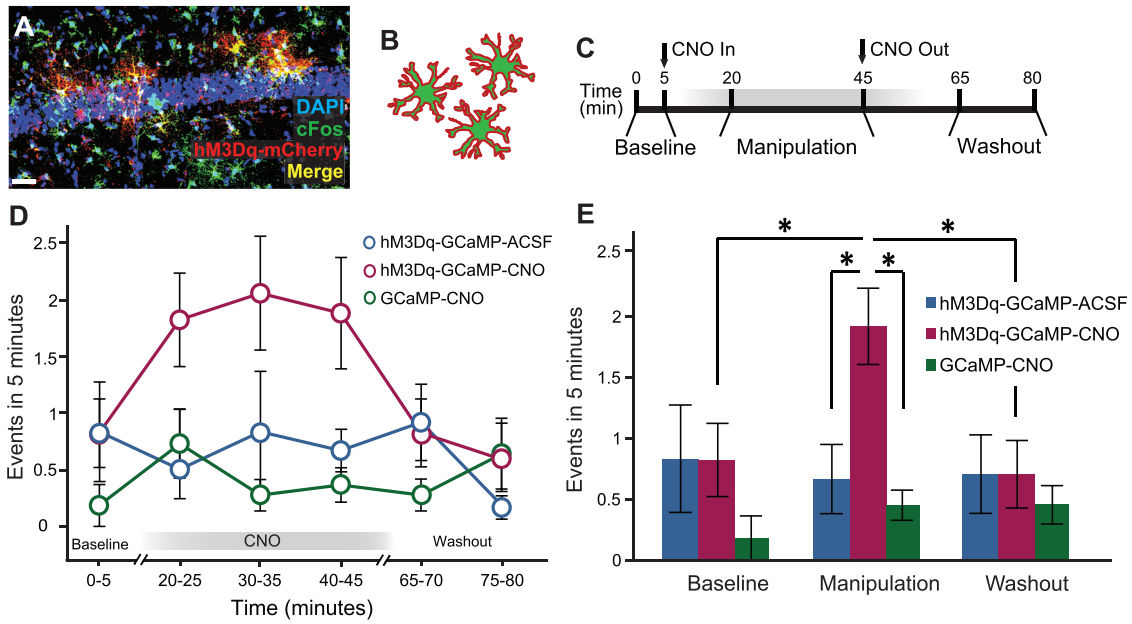

Figure S1. Long-Term Chemogenetic Activation of CA1 Astrocytes, Related to Figure 1

(A and B) CA1 astrocytes co-expressing hM3Dq-mCherry in their membranes and GCaMP6f in their cytoplasm (scale bar 30 μm) were imaged.

(C) 2-photon imaging was performed for 5 minutes before drug application (Baseline), and then the drug was applied. 15 minutes later, activity was imaged 3 times for 5 minutes with a 5 minutes interval between imaging sessions. The drug was then washed out, and 20 minutes later two 5 minutes imaging session, with a 5 minutes interval were performed.

(D and E) CNO application to hM3Dq-expressing slices (crimson) significantly increased the number of astrocytic events, compared to hM3Dq slices treated with ACSF (blue) ($p < 0.005$), to CNO application to slices with no hM3Dq (green) ($p < 0.001$), and to CNO baseline ($p < 0.005$) and CNO washout ($p < 0.0005$). Activity after CNO washout returned to baseline levels.

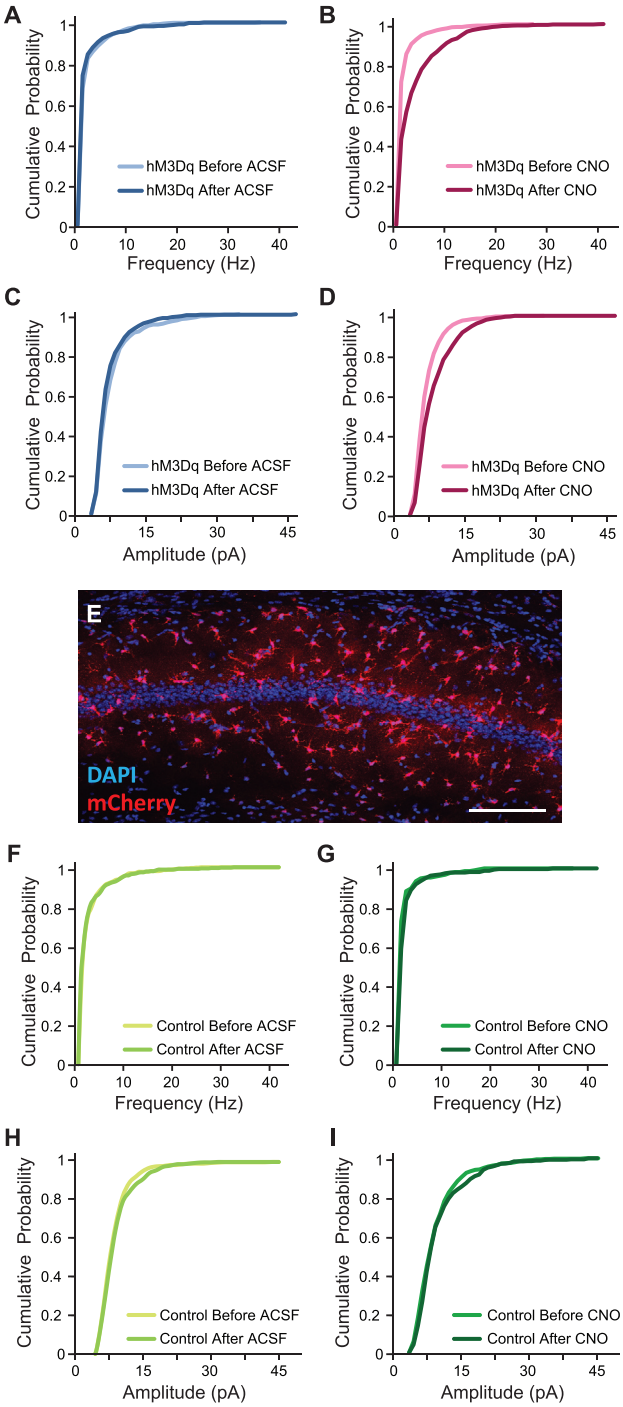

Figure S2. Astrocytic Activation Increases Spontaneous Neuronal Activity, Related to Figure 2

(A) No change in the frequency of spontaneous miniature events was observed in hM3Dq mice before and after ACSF application.

(B) A significant increase in mEPSC frequency was observed after, compared to before, CNO application in hM3Dq slices ($p < 0.001$).

(C) No change in the amplitude of spontaneous miniature events was observed in hM3Dq mice before and after ACSF application.

(D) A significant increase in mEPSC amplitude was observed after, compared to before, CNO application in hM3Dq slices ($p < 0.001$).

(E) Bilateral double injection of AAV8-GFAP-mCherry resulted in mCherry expression in CA1 astrocytes. Scale bar 100 μm. Whole-cell voltage-clamp recordings from CA1 hippocampal neurons surrounded by mCherry expressing astrocytes were performed before and after ACSF or CNO bath application (4 slices, from 2 mice and 4 slices from 3 mice, respectively).

(F–I) Neither ACSF nor CNO in mCherry expressing slices had any effect on either the frequency (F and G) or the amplitude (H and I) of spontaneous miniature events.

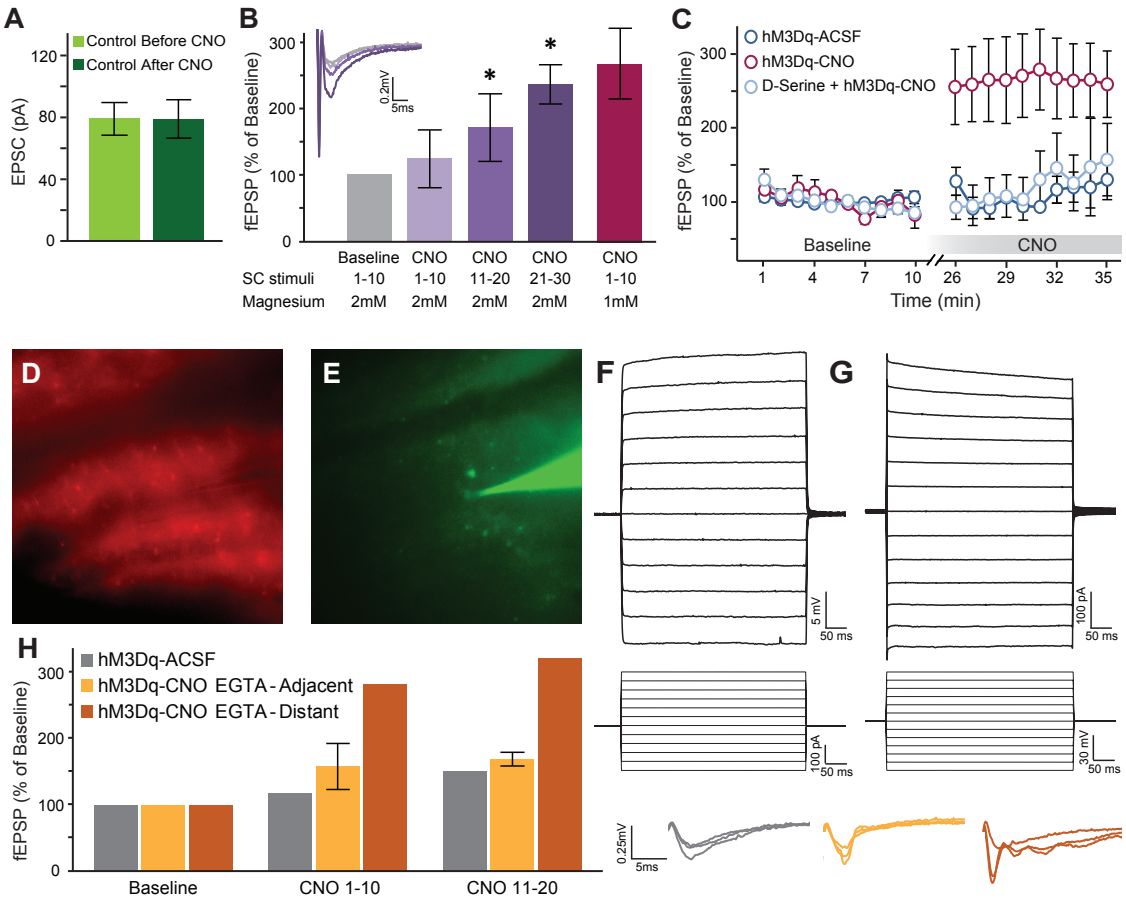

Figure S3. *De Novo* Potentiation Induced by Astrocytic Activation Is Occluded by D-Serine and Blocked by Ca^{2+} Chelation in Astrocytes, Related to Figure 3

(A) CNO application per se has no effect on evoked EPSCs in response to Schaffer Collaterals (SC) stimulation in mCherry-expressing slices.

(B) Astrocytic activation by CNO in the presence of 2mM magnesium in the recording chamber induced a > 130% potentiation in evoked fEPSP amplitude compared to slices from the same mice treated with ACSF, but required more SC stimulations or time to reach that effect, compared to the same manipulation performed with 1mM Magnesium (n = 3 slices from 3 mice; Time effect $F(3,8.1) = 5.85$, $p < 0.02$; Pairwise comparisons: Baseline versus 11-20 stimuli, $p < 0.05$; Baseline versus 21-30 stimuli, $p < 0.005$; 1-10 versus 21-30 stimuli, $p < 0.05$). Representative traces are presented in corresponding colors.

(C) Astrocytic activation by CNO failed to induce synaptic potentiation when 10 μM D-Serine was present in the recording bath (n = 7 slices from 3 mice).

(D–H) blocking Ca^{2+} increase in astrocytes prevents CNO-induced neuronal potentiation: In an area of hM3Dq-expressing (red) astrocytes (D), an astrocyte was patched with an internal solution containing the Ca^{2+} chelator EGTA and Alexafluor488 (green), which then diffused into neighboring astrocytes (E). We verified that the patched cells are astrocytes based on morphology, and on their non-excitable responses to stimulation in both current-clamp and voltage clamp. (F and G) Specifically, we injected step current in steps of 100 pA from −500 pA to +500 pA (F), and step voltage in 5mV steps, from −90 mV to +90 mV (G), and recorded typical non-excitable responses. When astrocytic activity was blocked in a group of astrocytes adjacent to the field recording site (n = 3 slices from 3 mice) only a minimal potentiation compared to ACSF-treatment was observed. (H) When the field response was recorded at a distant site from the blocked astrocytes, a full potentiation to > 250% of baseline was observed. Representative traces are presented in corresponding colors. Data presented as mean ± SEM.

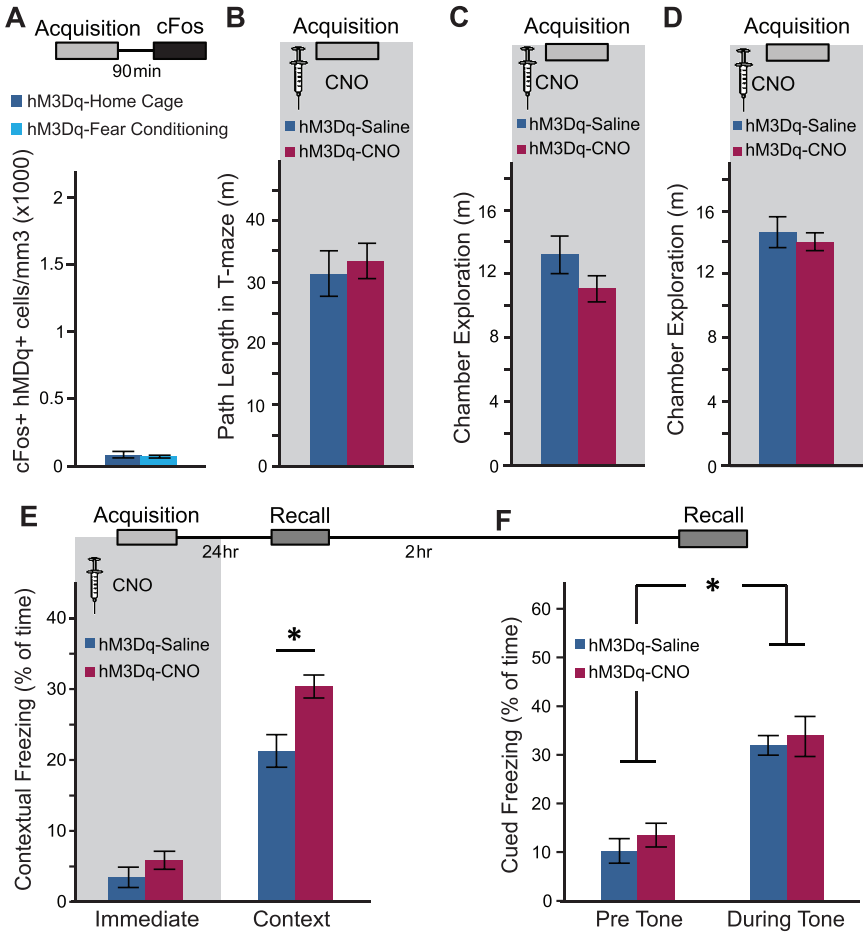

Figure S4. The Effects of Astrocytic Activation Are Limited to Hippocampal-Dependent Memory, Related to Figure 4

(A) Fear conditioning did not increase c-Fos expression in astrocytes compared to home-cage housing.

(B) Mice expressing hM3Dq in their CA1 astrocytes were injected with either saline (n = 7) or CNO (n = 7) 30 minutes before T-maze training.

(C) CNO application had no effect on exploration of the maze. Similarly, CNO had no effect on the exploration of the FC cage before conditioning. To replicate the results presented in Figures 4E and 4F, mice expressing hM3Dq in their CA1 astrocytes were injected with either saline (n = 8) or CNO (n = 10) 30 minutes before fear conditioning acquisition.

(D and E) CNO application did not affect the exploration of the conditioning cage (D) but resulted in a > 40% improvement in contextual freezing in CNO-treated mice tested one day later, compared to saline treated controls ($p < 0.005$) (E).

(F) No effect on auditory-cued memory was observed, with both groups showing increased freezing during tone presentation ($p < 0.00001$). Data presented as mean ± SEM.

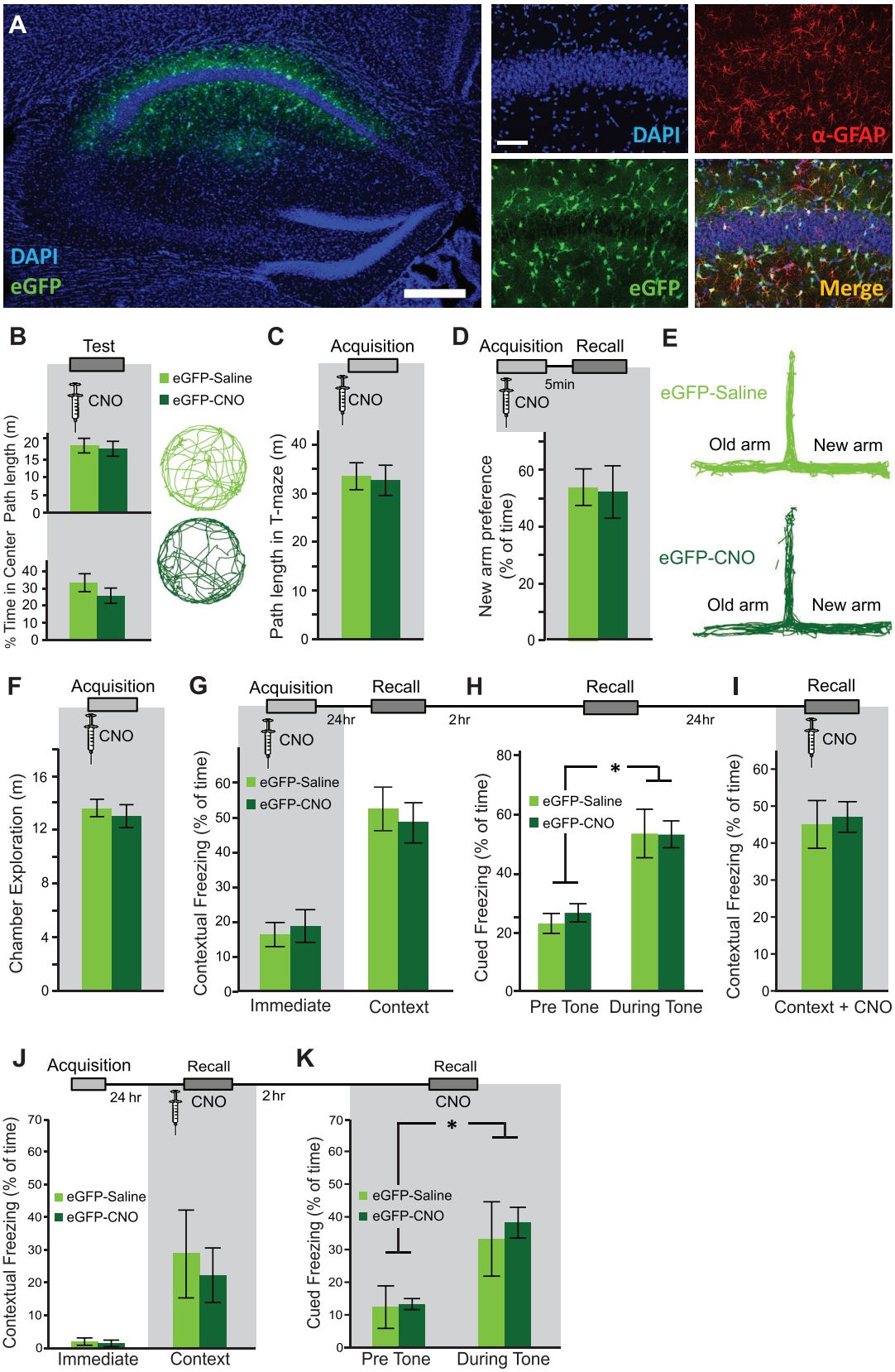

(legend on next page)

Figure S5. CNO Application Itself Has No Effect on Memory, Related to Figure 4

(A) Bilateral double injection of AAV8-GFAP-eGFP resulted in eGFP expression in CA1 astrocytes only. Scale bar – left 300 μm, right 50 μm.

(B) In a novel environment, saline-treated (n = 7) and CNO-treated (n = 7) eGFP mice explored the field with similar path lengths (top) and there was no effect on anxiety (bottom), as the percent of time that saline and CNO treated mice spent in the center of the open field was similar. Representative exploration traces are presented.

(C and D) Saline-treated (n = 7) and CNO-treated (n = 7) eGFP mice explored the T-maze with similar path lengths (C) and there was no effect on new arm recognition (D). (E) Representative exploration traces. Mice expressing eGFP in their CA1 astrocytes were injected with either saline (n = 7) or CNO (n = 7) 30min before fear conditioning acquisition.

(F–H) CNO administration before training to eGFP-expressing mice had no effect on exploration of the conditioning chamber (F) contextual memory (G) or auditory cued memory (H) one day later.

(I) CNO administration during recall on the next day also had no effect on retrieval.

(J and K) When administered during recall only, CNO administration to eGFP-expressing mice (n = 4) had no effect on contextual or auditory-cued memory compared to saline injected mice (n = 4). Data presented as mean ± SEM.

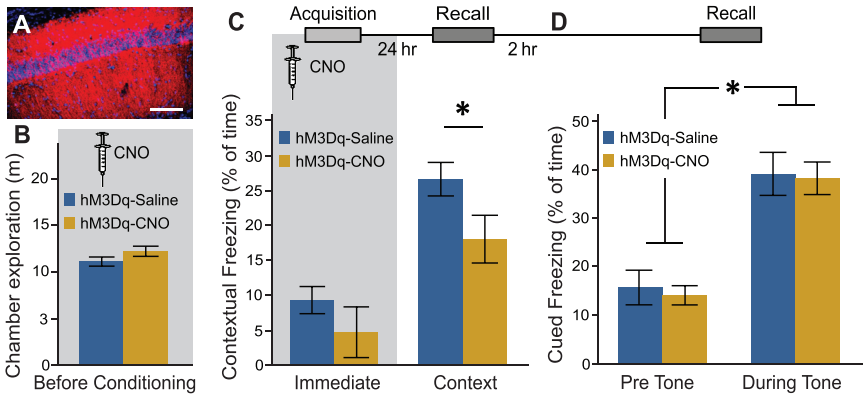

Figure S6. Mild Neuronal Activation Impairs Memory Performance, Related to Figure 5

(A) hM3Dq was expressed in CA1 neurons (Scale bar 100μm). Mice expressing hM3Dq in their CA1 neurons were injected with either saline (n = 6) or a low dose of CNO (0.5mg/kg; n = 6) 30min before fear conditioning acquisition.

(B) Neuronal activation had no adverse effect on exploratory behavior in the conditioning cage.

(C) CNO application before training induced a 55% decrease in contextual freezing in CNO-treated mice tested 24 hours later, compared to saline treated controls ($p < 0.05$).

(D) Neuronal activation in CA1 had no effect on auditory-cued freezing in a novel context, with both groups showing increased freezing during tone presentation ($p < 0.00001$). Data presented as mean ± SEM.

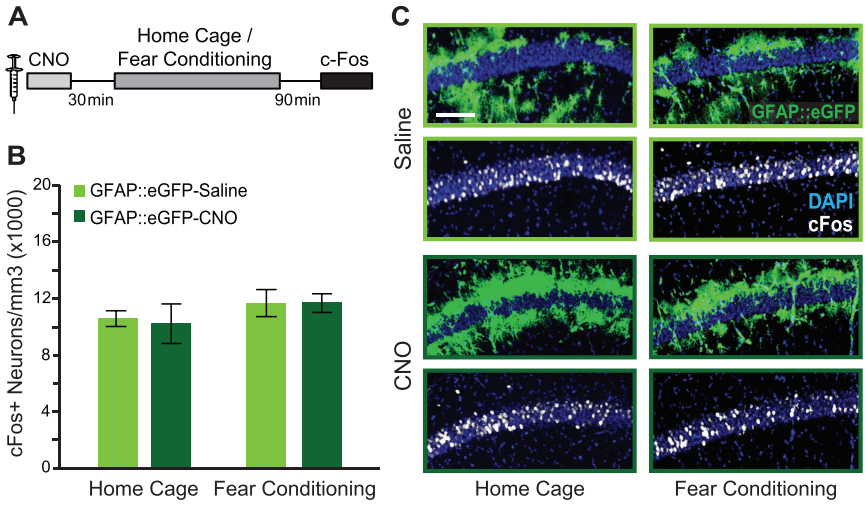

Figure S7. CNO Application by Itself Has No Effect on Neuronal Activity, Related to Figure 6

(A) CNO was administered to either home-caged or fear-conditioned AAV8-GFAP-eGFP mice.

(B) CNO application had no effect on neuronal activity, as measured by cFos expression, regardless of memory acquisition.

(C) Representative cFos expression images are shown (GFAP-eGFP in green, nuclei in blue, cFos in white; Scale bar 100μm). Data presented as mean ± SEM.